

Check for updates



SmartBot



MEMS: The Sensory Nervous System for Embodied AI Robots

Xu Zhou^{1,2} | Dongsheng Li¹ | Shuhan He^{3,4} | Mengyao Xiao^{3,4} | Zhouli Sui^{3,4} | Fusheng Zha² | Lining Sun^{1,2} | Chengkuo Lee^{3,4} | Huicong Liu¹

¹School of Mechanical and Electrical Engineering, Jiangsu Key Laboratory of Embodied Intelligence Robot Technology, Soochow University, Suzhou, China | ²State Key Laboratory of Robotics and System, Harbin Institute of Technology, Harbin, China | ³Department of Electrical and Computer Engineering, National University of Singapore, Singapore, Singapore | 4Center for Intelligent Sensors and MEMS (CISM), National University of Singapore, Singapore, Singapore

Correspondence: Lining Sun (Insun@hit.edu.cn) | Chengkuo Lee (elelc@nus.edu.sg) | Huicong Liu (hcliu078@suda.edu.cn)

Received: 6 July 2025 | Revised: 11 September 2025 | Accepted: 13 September 2025

Funding: This study was supported by the Natural Science Foundation of Jiangsu Province for Distinguished Young Scholars (Grant BK20220056) and the National Natural Science Foundation of China (Grant 52475599).

Keywords: embodied AI | MEMS technology | perception | robotics

ABSTRACT

The rise of embodied artificial intelligence (embodied AI) marks a pivotal shift in AI, moving it from the digital realm into the physical world. This transition aims to create autonomous robots capable of perceiving, reasoning, and acting in complex unstructured environments. Achieving this goal demands unprecedented capabilities for robots to comprehensively perceive both their external surroundings and internal states. However, traditional sensors cannot meet the requirement of robotic perception systems due to limitations in size and power consumption. In this context, micro-electromechanical system (MEMS) technology emerges as a critical enabler for advancing next-generation robotic perception capabilities. Its core advantages, including miniaturization, low power consumption, high integration, and cost-effectiveness, make it ideal for this role. This review provides a comprehensive overview of the latest advancements in MEMS sensing technologies specifically designed for embodied AI robots. By integrating diverse MEMS sensors, such as those for ranging, inertia, tactile, hearing, and olfaction, robots can achieve rich multimodal perception. These highly integrated sensing systems provide a robust technological foundation for robot applications in various fields, demonstrating the immense potential of MEMS technology in promoting autonomy, safety, and interactive capabilities in robots. In essence, the future of embodied AI will be built upon a powerful symbiosis: MEMS providing the rich semantic-aware 'sensory neurons' and AI models providing the 'cognitive brain'. This fusion promises to usher in an era of truly perceptive and intelligent machines.

1 | Introduction

The convergence of artificial intelligence (AI) and robotics has heralded a new era of embodied AI, a paradigm shift that moves AI from digital confines into the physical world [1]. Unlike traditional AI systems that process disembodied data, embodied agents, such as autonomous robots [2, 3], are designed to perceive, reason, and act within complex unstructured environments. The ultimate goal is to create machines capable of performing sophisticated tasks with human-like dexterity and adaptability from autonomous driving and industrial automation to in-home assistance and surgical operations [4-7]. This ambition places an unprecedented demand on the robot's ability to comprehensively understand its surroundings and its own state.

Xu Zhou and Dongsheng Li have contributed equally to this work.

This is an open access article under the terms of the Creative Commons Attribution License, which permits use, distribution and reproduction in any medium, provided the original work is properly

© 2025 The Author(s). SmartBot published by John Wiley & Sons Australia, Ltd on behalf of Harbin Institute of Technology.

SmartBot, 2025; 1:e70004 https://doi.org/10.1002/smb2.70004 The specific perceptual requirements are dictated by the robot's operating environment and intended tasks as shown in Figure 1. For instance, in industrial logistics or autonomous driving, a robot must navigate dynamic cluttered spaces [11, 12]. This necessitates a sophisticated 3D environmental awareness for mapping and collision avoidance, primarily furnished by ranging sensors, such as LiDAR and ultrasonic array, coupled with

inertial sensors to precisely track its own motion and orientation, especially in GPS-denied areas [13]. In the delicate context of medical robotics, a surgical robot assisting in minimally invasive procedures must not only see but also "feel". It relies on highly sensitive force and tactile sensors at its end-effector to differentiate between healthy and diseased tissue or to apply precise tension during suturing [14]. Similarly, for human-robot

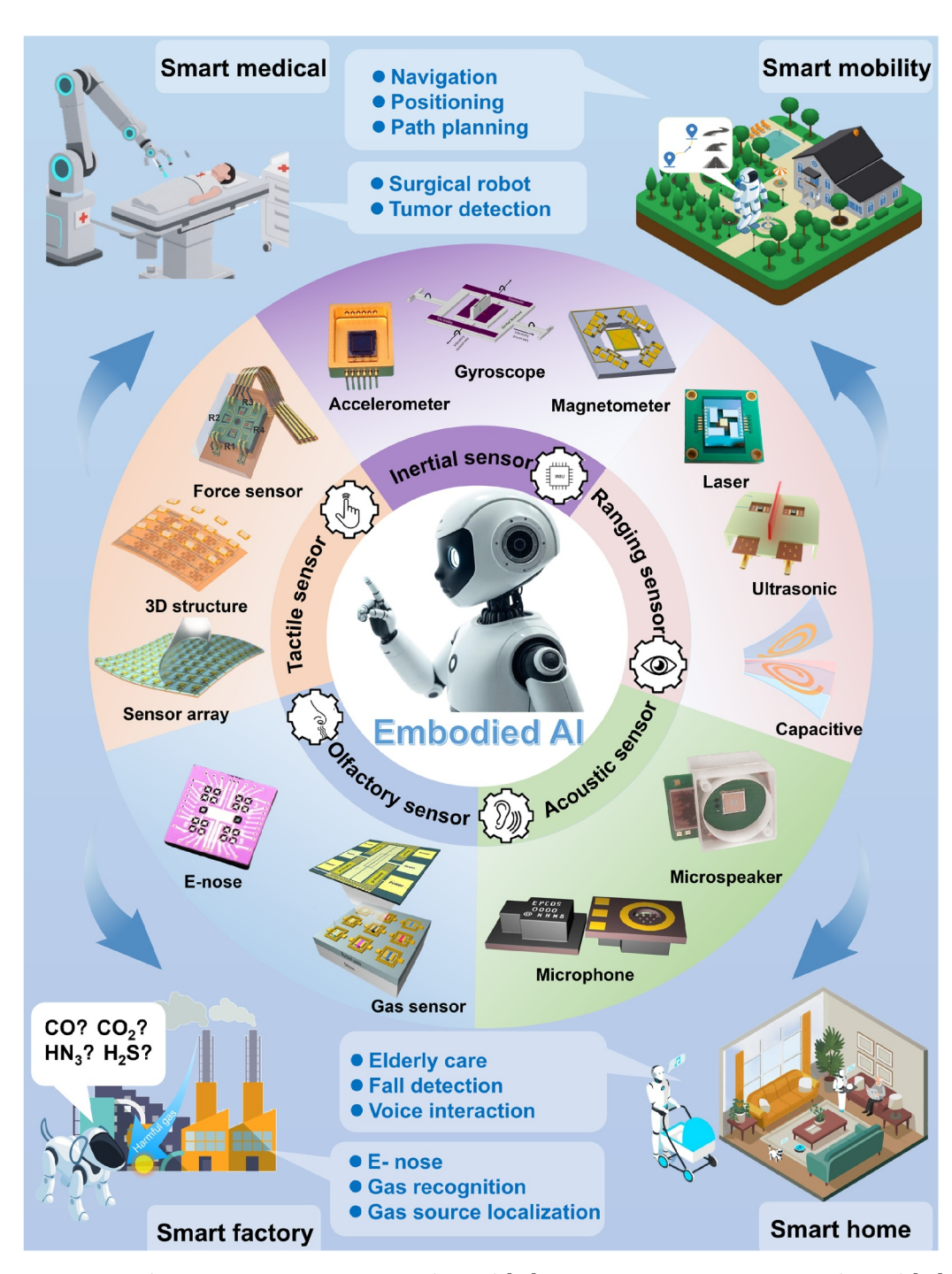


FIGURE 1 | MEMS sensors of embodied AI robots. Reproduced from ref. [21]. Copyright 2019 MDPI. Reproduced from ref. [22]. Copyright 2022 MDPI. Reproduced from ref. [23]. Copyright 2024 Springer Nature. Reproduced from ref. [24]. Copyright 2023 Wiley-VCH GmbH. Reproduced from ref. [25]. CC BY 4.0. Reproduced from ref. [26]. Copyright 2022 American Chemical Society. Reproduced from ref. [27]. Copyright 2024 Springer Nature. Reproduced from ref. [28]. CC BY 4.0. Reproduced from ref. [29]. Copyright 2010 Springer Nature. Reproduced from ref. [30]. Copyright 2023 IEEE. Reproduced from ref. [8]. Copyright 2022 American Chemical Society. Reproduced from ref. [9]. Copyright 2023 American Chemical Society. Reproduced from ref. [10]. Copyright 2023 MDPI.

interaction in a home-care or collaborative manufacturing setting, a robot requires proximity and tactile sensors to ensure safe physical contact, alongside microphones for seamless voice-based communication. Furthermore, in extreme environments, such as disaster response or military reconnaissance, a search-and-rescue robot must navigate treacherous unstable terrain using robust inertial measurement units (IMUs) and ranging sensors [15]. Simultaneously, it may employ microphones to detect faint sounds of survivors buried under rubble and olfactory sensors to identify hazardous chemical leaks, thus providing critical intelligence that is beyond human sensory limits. These scenarios underscore the critical need for a rich multimodal sensory suite to enable robust and intelligent robotic behavior.

Although these sensing modalities are conceptually established, their physical realization at the scale and performance required by modern robotics presents a formidable challenge. Traditional approaches to fabricating these sensors often create a critical bottleneck. High-performance systems, such as tactical-grade IMU or mechanical scanning LiDAR, are typically bulky, power-hungry, and prohibitively expensive. Conversely, their lower-cost alternatives have historically suffered from inadequate performance, stability, and integration density. This fundamental trade-off has long hindered the development of robots with the dense, distributed, and high-fidelity sensory systems needed for true autonomy. Herein, micro-electromechanical system (MEMS) technology emerges as the key to breaking this impasse. Characterized by its profound miniaturization, low power consumption, high integration density, and cost-effective batch fabrication, MEMS technology is ideally suited to serve as the scalable high-performance sensory backbone for next-generation robots [16-20]. By integrating micromechanical structures with electronic circuits on a single chip, MEMS sensors provide a powerful and versatile toolkit to endow robots with sophisticated perceptual capabilities.

To this end, this review provides a comprehensive overview of the state-of-the-art in MEMS sensing technologies tailored for embodied AI robots. It systematically surveys the fundamental principles, recent technological breakthroughs, and critical robotic applications of several key MEMS sensor categories. The document is structured as follows: it begins with MEMS ranging sensors that enable environmental mapping and obstacle avoidance. Subsequently, it delves into MEMS inertial sensors, the core components for attitude estimation and navigation. The discussion then explores MEMS force and tactile sensors, which are crucial for dexterous manipulation and safe interaction. Finally, it touches upon other emerging modalities, such as MEMS microphones and olfactory sensors, that further enrich robotic perception. By synthesizing advancements across these domains, this review aims to provide researchers in both the MEMS and robotics communities with a holistic understanding of the current landscape and to illuminate future directions for developing the advanced sensory systems that will bring embodied AI to life.

2 | Visual Perception

Accurate environmental perception is a cornerstone of robotic intelligence, enabling essential functionalities such as autonomous

navigation, object manipulation, and safe human-robot interaction. Central to this perceptual capability are ranging sensors, which measure the distance to surrounding objects. The advent of MEMS technology has revolutionized this domain by enabling the production of ranging sensors that are miniaturized, low-power, and cost-effective. These sensors function by monitoring distance-dependent alterations in their micromechanical structures, such as deformation or vibrational modes, or through characterizing the propagation dynamics of emitted waves. Based on their underlying physical principles, the most prominent MEMS ranging technologies for robotics include laser-based, ultrasonic, and capacitive sensing. This technological diversity provides a versatile toolkit of perception solutions, positioning MEMS as a key enabler for the next generation of intelligent robots.

2.1 | MEMS Laser Ranging Sensors

Laser ranging calculates the distance between objects and sensors by emitting laser beams to target surfaces and analyzing reflected signals. LiDAR, as a representative laser ranging technology, has been widely adopted in robotic environmental perception, autonomous navigation, and obstacle detection. The current mainstream test is time-of-flight (ToF) technology. The ToF technology determines target distances by measuring time delay between emitted laser pulse and returned echo, favored for its rapid response and high precision. Building on this foundation, MEMS laser ranging sensors utilize miniaturized laser sources and micromirrors to achieve high-precision long-distance measurements. This technology offers a compelling set of advantages, including high accuracy (often at the millimeter level for short ranges), long range (easily exceeding 100 m), and noncontact measurement. Furthermore, MEMS integration drastically reduces the size, power consumption, and cost of these systems, making them viable for portable applications. Compared to conventional LiDAR systems, these sensors exhibit superior advantages in power efficiency, integration density, and resolution, making them particularly suitable for dynamic scenarios.

Research on MEMS laser ranging sensors is extensive. As shown in Figure 2a, based on motion axes, they are categorized into 1D and 2D MEMS mirrors. The 1D MEMS mirror enables efficient unidirectional scanning via a single motion axis, whereas the 2D MEMS mirror counterpart achieves full-field coverage through coordinated dual-axis actuation. For 1D MEMS mirrors, Bascetta et al. proposed two distance feedback methods [35], geometry consistent trajectory and time consistent trajectory, to apply laser ranging to robot obstacle avoidance. Chen et al. proposed an ultratiny line laser range sensor with a precision deviation of less than 2 cm [43], which is used for environmental detection in miniature robots. Furthermore, researchers have achieved longdistance laser imaging using a 2D MEMS mirror. Yang et al. proposed a 360° LiDAR system based on a MEMS mirror that achieves a high angular resolution of $0.07^{\circ} \times 0.027^{\circ}$ [44]. This enhances the panoramic scanning and imaging capabilities of the LiDAR system, providing more precise 3D scanning applications for robotic navigation. Trocha et al. designed a soliton-comb ranging system and integrated it with chip-scale nanophotonic phased arrays [39], achieving an ultra-fast acquisition rate of 100 MHz, as illustrated in Figure 2b. This system also reduced the

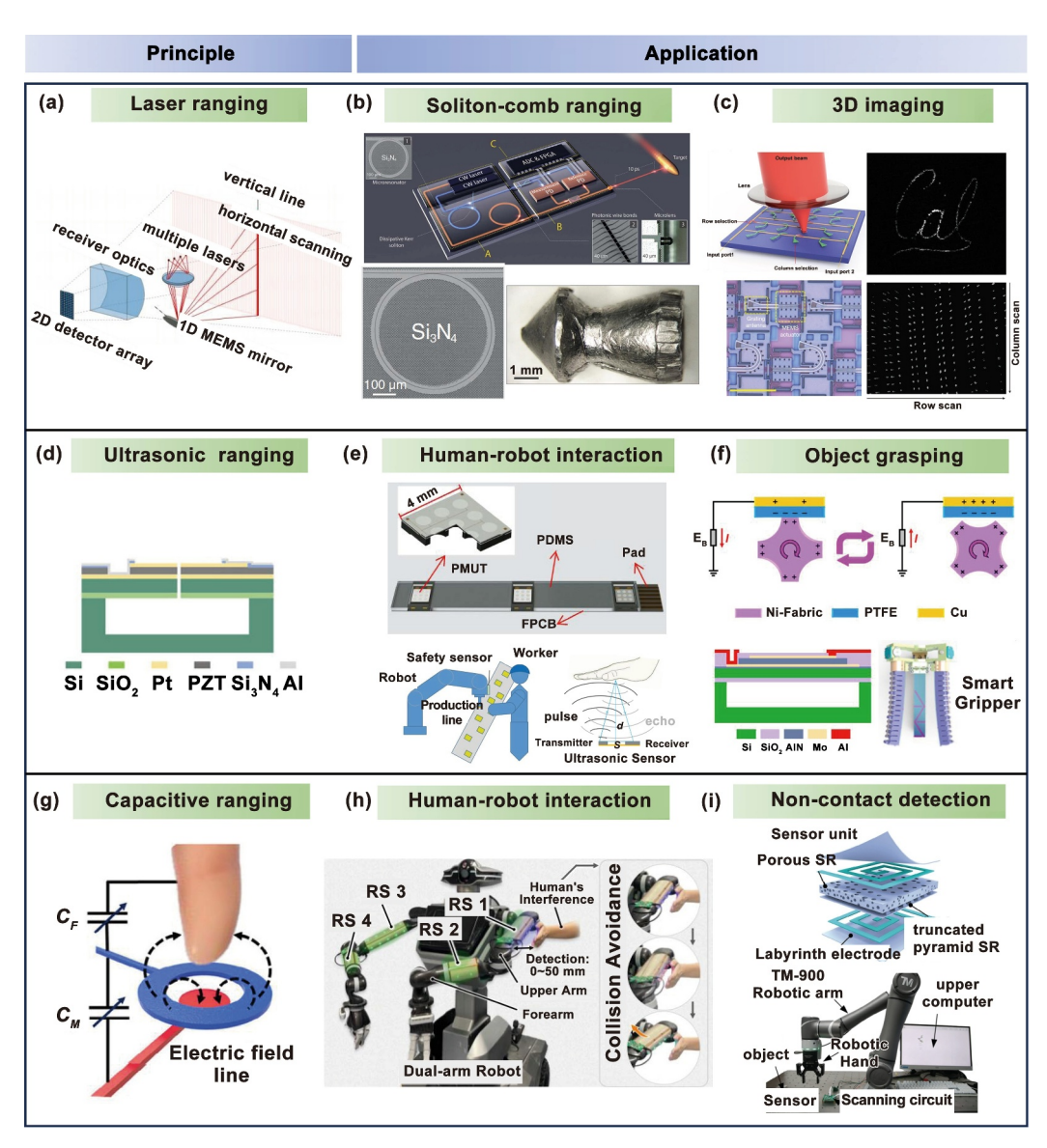


FIGURE 2 | MEMS ranging sensors. (a) Principle of laser ranging sensors. Reproduced from ref. [38]. Copyright 2020 MDPI. (b) Ultrafast optical ranging using microresonator soliton frequency combs. Reproduced from ref. [39]. Copyright 2018 The American Association for the Advancement of Science. (c) MEMS LiDAR achieves 3D imaging. Reproduced from ref. [40]. Copyright 2022 Springer Nature. (d) Principle of ultrasonic ranging sensors. Reproduced from ref. [32]. Copyright 2025 Wiley-VCH GmbH. (e) Ultrasonic proximity sensing skin for robot safety control by PMUTs. Reproduced from ref. [41]. Copyright 2022 IEEE. (f) Soft robotic perception system with ultrasonic auto-positioning. Reproduced from ref. [9]. Copyright 2023 American Chemical Society. (g) Principle of capacitive ranging sensors. Reproduced from ref. [32]. Copyright 2024 Wiley-VCH GmbH. (h) Human-robot interaction. Reproduced from ref. [33]. Copyright 2024 IEEE. (i) High-sensitivity noncontact detection. Reproduced from ref. [42]. Copyright 2024 Wiley-VCH GmbH.

Allan deviation to 12 nm, making a compact high-speed ranging system possible for large-scale applications. Zolfaghari et al. achieved ultrawide scanning angles by designing a folding mechanism that enables the cascading of multiple piezoelectric MEMS devices [45]. Zhang et al. fabricated a MEMS LiDAR with a wide field of view on a $10 \times 11~\text{mm}^2$ silicon photonic chip [40]. As shown in Figure 2c, this device has 16,384 pixels and achieves 3D imaging with a distance resolution of 1.7 cm. In summary, through structural innovations and multiactuation synergies, MEMS laser ranging sensors have achieved breakthroughs in high resolution, wide-angle scanning, and long-range detection. These advancements provide critical technical support for three-dimension environmental perception in intelligent robotics and autonomous driving applications.

The dense point clouds generated by MEMS LiDAR are particularly amenable to processing by deep learning models, such as PointNet++ or occupancy grid mapping algorithms, enabling sophisticated functions, such as semantic segmentation of the environment and dynamic object tracking, which are critical for autonomous navigation.

2.2 | MEMS Ultrasonic Ranging Sensors

MEMS ultrasonic ranging sensors generate mechanical vibrations via MEMS-structured diaphragms to emit ultrasonic signals. Reflected signals from targets act on the diaphragm,

converting mechanical vibrations into voltage outputs. The predominant measurement method remains ToF technology, which calculates distances by measuring the time delay between signal emission and reception, combined with sound velocity. Compared to laser ranging, ultrasonic systems exhibit shorter detection ranges due to slower sound propagation but demonstrate superior immunity to electromagnetic and environmental interference, making them ideal for short-range applications.

Based on energy conversion mechanisms, MEMS ultrasonic sensors are categorized into piezoelectric micromachined ultrasonic transducers (PMUTs) and capacitive micromachined ultrasonic transducers (CMUTs). PMUTs leverage the inverse/positive piezoelectric effects of materials for ultrasound generation and reception, offering high sensitivity and ease of integration. CMUTs rely on capacitance variations between diaphragm and substrate for signal transduction, providing broader bandwidth. These innovations provide new approaches to enhance robotic environmental perception. As shown in Figure 2d, with advantages in short-range precision and environmental robustness, MEMS ultrasonic sensors are widely deployed in indoor robotics, proximity sensing, and obstacle avoidance. Luo et al. proposed a broadband ultrasonic rangefinder with merits of a small blind area and high accuracy [46]. This device features an ultrasmall blind zone of 5 mm and an ultrahigh accuracy with an error of 0.3 mm, making it suitable for short-distance ranging. Addressing robotic safety, Tong et al. designed a flexible ultrasonic proximity-sensing skin integrated onto robotic arms (Figure 2e), significantly improving collision avoidance in human-robot collaboration [41]. Shi et al. integrated ultrasonic and triboelectric sensors for soft robotic object grasping (Figure 2f), achieving both remote target localization and multimodal cognitive capabilities [9]. Emerging applications include curved-surface PMUTs for conformal object detection and hybrid optical-PMUT systems for intracavity imaging in continuum robots [34]. Through continuous advancements, MEMS ultrasonic sensors have become pivotal in robotic navigation, safety assurance, and dynamic perception, driving intelligent upgrades in robotic systems.

2.3 | MEMS Capacitive Ranging Sensors

MEMS capacitive ranging sensors measure distance through capacitance variations between objects and sensor electrodes. The principle of a MEMS capacitive ranging sensor is to utilize the change in distance between the two plates of a capacitor caused by a physical quantity under measurement. This change alters the capacitance value, which is then amplified, linearized, and converted into a standard electrical signal output by a precision integrated circuit. This technology represents a seamless integration of mechanical motion and electronic signals in a miniaturized sensor. This technology represents a seamless integration of mechanical motion and electronic signals in a miniaturized sensor. This approach endows MEMS capacitive sensors with exceptional advantages, primarily extremely high precision and resolution (capable of detecting sub-nanometer changes), low power consumption, and minimal heat generation. Their simple structure also makes them robust, costeffective, and resistant to environmental light interference. However, the fundamental operating principle also dictates their main limitations. They are inherently short-range devices, typically effective from a few millimeters up to a few centimeters. Their performance is also highly susceptible to environmental interference, such as humidity, temperature fluctuations, and the presence of dust, oil, or other contaminants. Additionally, they require precise calibration and can be sensitive to electromagnetic interference. Consequently, these sensors excel in scenarios requiring micron or nanometer-level accuracy over tiny distances. As shown in Figure 2g, when a conductor approaches an electrode, it is influenced by the external electric field generated by the electrode, inducing a charge distribution on its surface [36]. This change in charge distribution affects the existing free charge distribution on the electrode, thereby altering its self-capacitance. Unlike line-of-sight technologies like LiDAR and ultrasound, capacitive sensors excel in non-contact proximity detection of a wide range of materials, including insulators. This unique capability makes them an ideal complement, particularly for applications, such as hidden obstacle detection or safe human-robot interaction, where direct line-of-sight may be occluded. Different from conventional sensors, they detect both metallic and insulating materials [37], excelling in microdistance measurements for robotic proximity sensing and precision positioning.

As robotics advances toward intelligence and miniaturization, MEMS capacitive sensors play a critical role due to their high sensitivity, compactness, and low power consumption. They enhance robotic spatial perception through noncontact displacement detection, enabling applications from robotic arm positioning to tactile feedback and human-robot interaction. For autonomous mobile robots and drones, MEMS capacitive proximity sensors can penetrate insulating materials, such as paper and plastic by generating electric or magnetic fields, thereby enabling safe obstacle avoidance under non-line-of-sight conditions. Li et al. developed a flexible laser-patterned copper electrode sensor [31], achieving 200 mm detection ranges for battery-powered service robots. Such sensors penetrate non-metallic materials to identify hidden obstacles, complementing LiDAR's limitations in transparent object recognition. Li et al. designed a full-range proximitytactile sensing module that uses a capacitive sensor for short-range proximity sensing [32], achieving an ultrahigh accuracy of 96.47% and excellent stability. Additionally, capacitive sensors are widely used in the field of human-robot interaction. As shown in Figure 2h, Wang et al. designed a 6-DOF capacitive robot skin [33]. This skin uses a hierarchical proximity-sensing method to classify the sensing state and employs a distance-reduction and collisionavoidance-based velocity-generation method to achieve smooth and rapid velocity decay, ensuring safety and flexibility in humanrobot interaction. Researchers have extensively investigated capacitive microstructure sensors for robotic noncontact detection. For instance, as depicted in Figure 2i, Liu et al. proposed a labyrinth-patterned electrode to improve proximity sensing capabilities [42], which they applied to human-machine interaction interfaces. Similarly, Huang et al. introduced an Archimedean spiral electrode [8], which effectively increased the intensity and depth of the fringe field along the Z-axis. This innovation assists machines in precisely sensing objects throughout the entire process, from proximity to touch.

The noncontact capability and flexible design of MEMS capacitive sensors endow robots with human-like perception. With breakthroughs in materials and fabrication techniques, next-

generation sensors will evolve toward multimodal intelligence, propelling robotics toward higher autonomy, safety, and interactive capabilities.

2.4 | MEMS Ranging Sensors for Robots

A robot system, especially one based on closed-loop feedback control, relies on the strict implementation of real-time data processing and extremely low latency for its stable and efficient operation. This need stems from a dynamic closed-loop process: sensors must continuously and at a high frequency perceive the environment, such as detecting obstacles. The resulting data must then be processed and computed rapidly, ultimately driving actuators to make precise low-latency responses, with a required delay typically under 100 ms. This "sense-compute-act" closed loop must operate at high speed without interruption. MEMS sensors are fundamentally suited for these applications. The update rate for MEMS ranging sensors is typically designed to be higher than 1 kHz. This rapid dataflow is crucial for a robot to respond to its environment promptly and accurately. This demonstrates that the high data rate and low latency of MEMS sensors are more than just performance metrics. They are essential for achieving adaptive closed-loop control in practical applications. The ability of these sensors to provide high-speed low-latency data are critical for autonomous systems that must make split-second decisions. Additionally, MEMS ranging sensors can be designed to a millimeter-scale size, enabling either high-precision measurements of around 1 mm or large-range measurements of 2 m. For robotic sensing applications, different types of sensors are required depending on the specific application scenario. According to the results in Table 1, laser ranging sensors can achieve long-distance measurements and have a high recognition capability, making them suitable for obstacle avoidance in long-range measurement scenarios. When used for close-range measurements, their high precision can be applied to 3D imaging. Ultrasonic ranging sensors, due to their excellent anti-interference and distance-sensing capabilities, are more often used for environmental perception and safe operation. Capacitive ranging sensors have a relatively smaller measurement range but offer better sensitivity, making them more suitable for proximity sensing or human-machine interaction. This allows them to meet both the high-integration size requirements of robots and the varying measurement range demands.

3 | Inertial Perception And Course Perception

As one of the most representative products of MEMS technology, inertial sensors specialize in measuring acceleration,

angular velocity, and orientation changes. Compared with traditional counterparts, MEMS devices achieve a size reduction of over tenfold and power consumption lowered to milliwattlevel. This technological innovation enables the embedding of high-dynamics multidegree of freedom motion perception into diverse robotic platforms, allowing real-time attitude feedback via MEMS inertial sensors across applications ranging from microdrones to heavy-duty industrial robotic arms.

As shown in Figure 3a, MEMS inertial sensors primarily consist of accelerometers gyroscopes. On the other hand, magnetometer is a different type of sensor used to measure the strength and direction of a magnetic field. Its function is to provide a heading reference, typically by measuring the Earth's magnetic field, similar to a compass. By measuring the Earth's magnetic field, a magnetometer provides a stable external reference point. This allows robotic systems to determine their heading and correct for the long-term drift that plagues pure inertial navigation. Therefore, magnetometers are often used to complement inertial sensors, with the combination of the two enabling a high degree of accuracy and reliability. By measuring physical parameters, including acceleration, angular velocity, and magnetic fields, they enable realtime determination of object orientation. Robotic autonomy critically depends on precise proprioception—the sense of its own state and motion. MEMS inertial sensors form the very foundation of this capability. For instance, drones necessitate real-time monitoring of attitude angles during hovering to prevent overturning, while bipedal robots dynamically adjust their center-ofmass balance through acceleration data analysis during locomotion. Simultaneously, autonomous mobile robots operating in GPS-denied environments, such as warehouses, must depend on inertial navigation for precise positioning. MEMS inertial sensors directly address these needs: accelerometers detect linear dynamics, whereas gyroscopes capture rotational motion. When fused, their data provide a comprehensive 3D state estimation from orientation to velocity and displacement, which is crucial for robotic operation.

3.1 | Accelerometers

MEMS-based accelerometers represent one of the most mature and widely adopted MEMS technologies, enabling velocity and displacement estimation of moving objects through single and double integration. Based on operational principles, MEMS accelerometers are primarily categorized into capacitive, piezoresistive, piezoelectric, and resonant types [63]. Capacitive accelerometers detect acceleration through gap-varying capacitance between a fixed electrode and an elastic diaphragm [64].

TABLE 1 | Comparison of MEMS ranging sensors.

Ref.	Sensing mechanism	Dimension	Measurement range	Resolution
[35]	Laser	N/A	0.2–2 m	< 1 mm
[43]	Laser	$35\times27\times30~mm$	0.05-2 m	< 2 cm
[46]	Ultrasonic	Area:11 × 11 mm	< 0.25 m	< 0.3 mm
[41]	Ultrasonic	$4 \times 4 \times 0.5 \text{ mm}$	< 0.3 m	< 1 mm
[31]	Capacitive	N/A	< 0.02 m	1.7 cm
[32]	Capacitive	Φ 30 \times 9 mm	< 0.015 m	< 1 mm

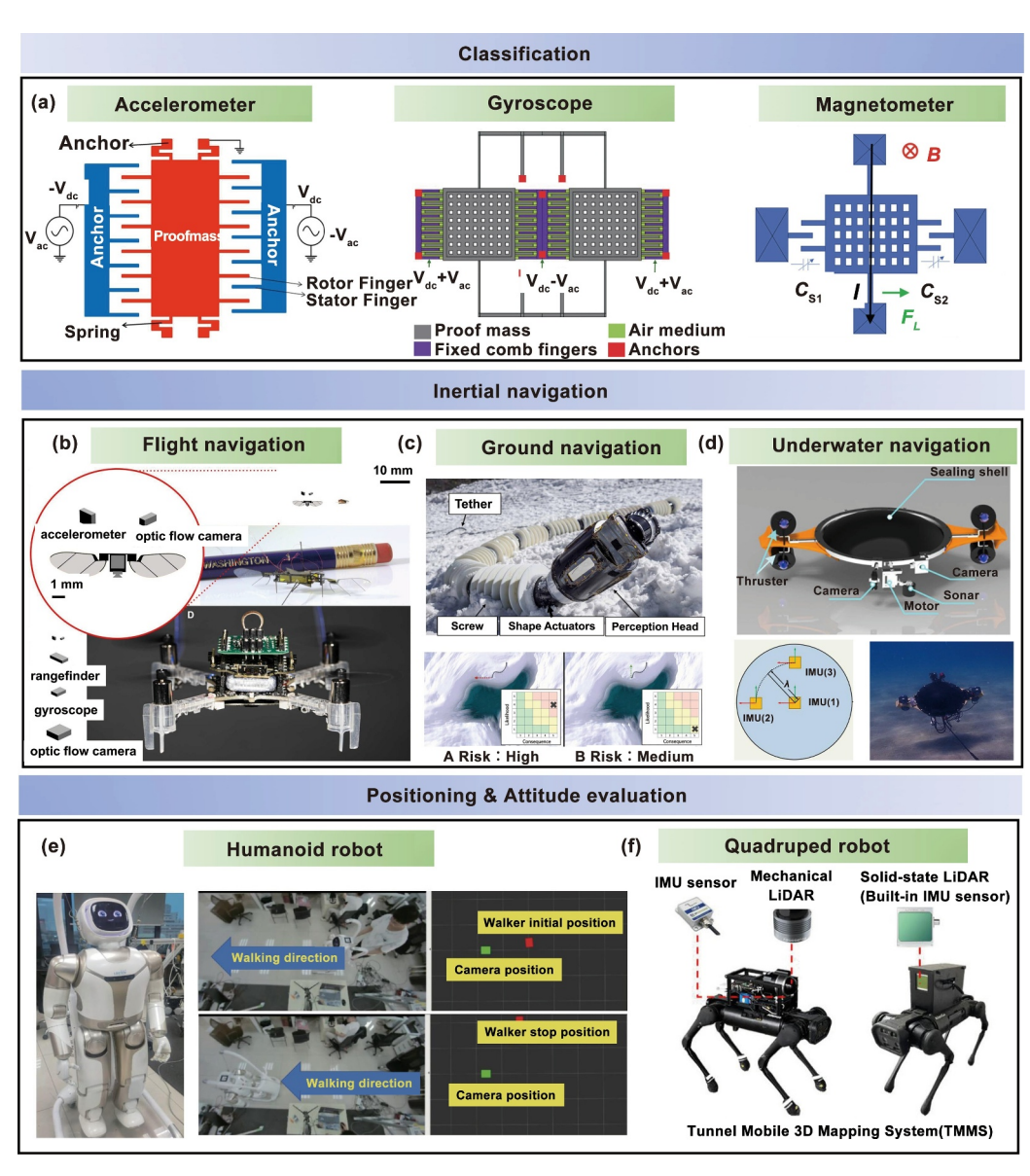


FIGURE 3 | MEMS inertial sensor. (a) Structure of typical MEMS accelerometer, gyroscope, and magnetometer. Reproduced from ref. [55]. Copyright 2019 Springer Nature. Reproduced from ref. [56]. Copyright 2025 Springer Nature. Reproduced from ref. [57]. Copyright 2022 Springer Nature. (b) A miniature accelerometer achieves inertial flight control for a 10-mg robot. Reproduced from ref. [58]. Copyright 2022 The American Association for the Advancement of Science. (c) Snake-like robot with IMU explores ice world [59]. Copyright 2024 The American Association for the Advancement of Science. (d) Underwater robots navigate using an IMU. Reproduced from ref. [60]. Copyright 2024 Springer Nature. (e) Positioning of humanoid robots. Reproduced from ref. [61]. Copyright 2025 Elsevier Ltd. (f) Attitude evaluation of quadruped robot. Reproduced from ref. [62]. Copyright 2025 Elsevier Ltd.

The diaphragm displacement under inertial forces alters capacitance, with advantages including high sensitivity, stable output, and environmental robustness. Piezoresistive accelerometers detect acceleration via resistance changes in doped silicon beams caused by inertial forces. Fabricated through silicon micromachining, they exhibit broad bandwidth but relatively lower sensitivity [65]. Piezoelectric accelerometers generate surface charges proportional to applied mechanical stress. When acceleration-induced vibrations act on a proof mass attached to piezoelectric elements, charge output correlates linearly with acceleration. Their high sensitivity, wide bandwidth, and low noise density make them ideal for vibration analysis in industrial machinery [66]. The resonant accelerometers detect acceleration by monitoring shifts in resonant frequency. When subjected to

external acceleration, the stress or mass distribution of the resonant structure changes, inducing a corresponding frequency deviation that enables the measurement of acceleration. [50]. Their exceptional sensitivity to microstrain makes them valuable for robotic fine motion control.

3.2 | Gyroscopes

MEMS gyroscopes detect rotational motion by measuring angular velocity, operating on the Coriolis effect principle: the apparent deflection of moving objects relative to earth's rotation [51]. A typical MEMS gyroscope operates by driving a proof

mass into oscillation along a primary axis (X-axis) using electrostatic, piezoelectric, or electromagnetic actuation. When the gyroscope rotates about its sensitive axis (Z-axis), the vibrating mass experiences a Coriolis force perpendicular to both the drive direction and rotation axis, inducing displacement along an orthogonal axis (Y-axis). The Coriolis force is expressed as follows:

$$F_c = -2m(\omega \times \nu),\tag{1}$$

where m represents the proof mass, ω denotes the angular velocity of the rotating system, and ν indicates the linear velocity of the mass.

The resultant displacement of the mass is detected via capacitive or piezoresistive sensing mechanisms, with subsequent signal processing generating electrical outputs proportional to angular velocity. These devices are critical for measuring and controlling robotic orientation, providing real-time angular velocity or attitude variation data.

3.3 | Magnetometers

Magnetometers convert variations in the magnetic properties of sensing elements induced by external factors, such as magnetic fields, electric currents, and mechanical stresses into measurable voltage or current signals, primarily used for estimating magnetic field strength and direction. Conventional magnetometers predominantly rely on the Hall effect, magnetoresistance effect, or magnetoresistance effect, whereas MEMS-based magnetometers are primarily constructed based on the Lorentz force principle. The operational mechanism involves the resonant frequency shift of vibrating microstructures under Lorentz forces when subjected to a magnetic field. This shift is detected through capacitive or piezoresistive sensing to derive magnetic field information [52]. Owing to their high sensitivity, compact integration, and low power consumption, Lorentz force-based MEMS magnetometers have found applications in scenarios such as drone attitude control and robotic azimuth estimation.

3.4 | Applications

Based on the data presented in Table 2, MEMS inertial sensors are capable of meeting the navigation, positioning, and path-planning requirements of embodied AI robots due to their small size and high sensitivity. MEMS accelerometers have good linearity, enabling precise measurement of a robot's linear acceleration and vibration states, which provides data support for

motion control and anticollision functions. MEMS gyroscopes detect angular velocity based on the Coriolis effect. Their high sensitivity and fast dynamic response allow for real-time tracking of a robot's attitude changes, meeting the needs for precise steering and balance adjustment. MEMS magnetometers sense the direction of the Earth's magnetic field, providing an absolute heading reference for the robot and compensating for the cumulative errors in long-term inertial navigation. By fusing multimodal data from these three types of sensors, they collectively form the core sensing unit for a robot's navigation, positioning, and path planning, enabling autonomous obstacle avoidance, stable movement, and precise orientation in complex environments.

The true power of MEMS inertial sensors is unleashed when accelerometers, gyroscopes, and magnetometers are integrated into a single package—the IMU. Through sophisticated sensor fusion algorithms, the IMU provides a robust and continuous estimation of the robot's full 3D state, forming the backbone of modern robotic navigation and control. The navigation function of an IMU is demonstrated in various aspects of robotics, including aerial, ground, and underwater applications. Inspired by fruit flies, Fuller et al. proposed a gyroscope-free visual-inertial flight control method where a 2-mg accelerometer can achieve flight control for a 10-mg robot [58] as shown in Figure 3b. Compared to conventional hovering controllers, this approach reduces mass by more than 20 times and power consumption by more than 100 times. Vaquero's research team has studied IMU navigation for ground robots [59]. They developed a risk-aware autonomous robot that combines an IMU to safely and effectively navigate and perceive icy environments (Figure 3c), such as those on Enceladus, where surface geometry and physical characteristics are highly uncertain. Liu et al. also proposed a maneuverable underwater vehicle for nearseabed observations [60] as depicted in Figure 3d. Using IMU navigation and real-time path planning, this vehicle can quickly detect strong disturbances, such as turbulence and wall effects, enabling high-quality observations of the seabed environment from a distance of nearly 20 cm.

IMUs are widely used in humanoid and quadruped robots for applications such as localization, pose estimation, and path planning. For humanoid robot localization, Ma et al. designed a leg odometry algorithm based on forward kinematics and IMU feedback [61]. This method uses a Kalman filter to fuse kinematic information and IMU data, achieving high-precision, real-time localization for humanoid robots as depicted in Figure 3e. Its low hardware cost and high robustness provide a practical solution for the localization of legged robots in indoor environments. Zhang et al. proposed a 3D tunnel mapping system

TABLE 2 | Comparison of MEMS inertial sensors.

Ref.	Type	Sensing mechanism	Dimension	Resonant frequency	Linearity	Sensitivity
[53]	Accelerometer	Capacitive	Proof mass:2000 \times 500 μm	1506.58 Hz	0.03%-0.04%	21.3 mV/g
[54]	Accelerometer	Piezoresistive	$360\times300\times40~\mu m$	30 kHz	N/A	98 mV/g
[47]	Accelerometer	Piezoelectric	$2000\times2000\times450~\mu m$	3048.83 Hz	N/A	149.83 mV/g
[48]	Gyroscope	Piezoelectric	$5000\times5000\times25~\mu m$	12.14 kHz	N/A	N/A
[49]	Magnetometer	Capacitive	Beam:2000 × 30 × 50 μm	37.487 kHz	0.42%	214.2 mV/mT

for quadruped robots based on simultaneous localization and mapping (SLAM) [62]. This system uses an IMU to perform motion compensation and attitude constraints (Figure 3f), correcting errors caused by robot movement to achieve 3D scanning of tunnel environments.

In summary, from the sky to the deep sea, the IMU serves as the core sensing unit for navigation in various types of robots, continuously pushing the boundaries of robotic capabilities in complex, dynamic, and extreme environments.

4 | Tactile Perception

In complex and unstructured environments, robots necessitate precise perception of physical contact forces to achieve safe and dexterous manipulation. Force sensors and tactile sensors are core components forming this physical interaction perception capability. The primary function of force sensor is to precisely quantify the magnitude and direction of force vectors, including normal and shear forces, applied at a specific point or over a small area. Its output typically consists of discrete force or torque components. Conversely, tactile sensors more closely mimic the function of biological skin, aiming to acquire richer and more spatially distributed physical information at the contact interface. The core lies in perceiving the spatial distribution of pressure or force, often integrating the capabilities to detect object texture, roughness, slip status, and temperature. The working principles of these two types of sensors are primarily based on several core physical effects: piezoresistive, capacitive, piezoelectric, and triboelectric effects. Based on these principles, sensors are capable of converting mechanical stimuli into measurable electrical signals.

4.1 | MEMS Force And Tactile Sensors

Due to form factor constraints, embodied AI robots have more stringent requirements for sensor size and power consumption. On one hand, sensors for parts, such as joints and skin, are typically required to have excellent flexibility and integration. For instance, sensors integrated into joints must often fit into packages smaller than 10×10 mm with a profile under 2 mm, whereas flexible sensors for e-skin need to be ultra-thin, typically less than 100 microns, and withstand thousands of bending cycles. On the other hand, MEMS sensors have an inherent energy-saving property due to their microscopic size, which meets the robotic system's demands for high integration and low power consumption. A single MEMS-based IMU can operate at power levels as low as a few milliwatts (mW) or even hundreds of microwatts (µW), with sleep modes drawing mere microwatts. This extreme efficiency is critical for extending operational lifetime, ensuring that the entire perception subsystem does not become a dominant power load, thereby enabling continuous operation for hours or days on a single battery charge. MEMS technology provides a unified and robust technical foundation for the miniaturization, high precision, and array formation of both force and tactile sensors [67]. The core advantage of MEMS lies in utilizing micromachining processes to integrate delicate microstructures, such as microbeams,

micromembranes, micromasses, and microelectrode arrays, alongside signal processing circuits on the same chip or within a compact package. This technological approach significantly reduces sensor size, allowing them to be embedded in robot joints, dexterous end-effectors or integrated as distributed sensing units on the robot's surface skin, thus meeting the demands for robot miniaturization and high integration. Furthermore, MEMS technology enables the fabrication of microstructures with high consistency and sensitivity. It significantly enhances the accuracy, resolution, and response speed of force or torque measurements, which is particularly suitable for fine operations requiring microforce control, such as in minimally invasive surgery. Finally, MEMS technology is especially well-suited for manufacturing large-scale high-density sensing unit arrays, which is crucial for achieving high spatial resolution tactile perception. Through precise micromachining techniques, MEMS sensors can realize array arrangements of sensing units, providing robots with skin-like distributed tactile sensing capabilities.

MEMS force and tactile sensors can be classified into piezoresistive, capacitive, and electromagnetic types based on their
working principles. As shown in Figure 4a, MEMS piezoresistive sensors detect external forces by measuring the change
in resistance caused by material deformation. Liu's research
team has conducted related studies on piezoresistive force
sensing for minimally invasive surgery. The research team
designed a highly integrated MEMS piezoresistive 3D forcesensing module [24] (Figure 4b). Its miniaturized size allows
it to be integrated into the tips of various surgical instruments.
The sensitivity and measurement range can be adjusted for
different surgeries by changing the elastic layer. This design
addresses the lack of force feedback experienced by surgeons
during operations.

The research team from Sungkyunkwan University in Korea has conducted many innovative studies on sensing for minimally invasive surgery. As shown in Figure 4c, they proposed a new surgical forceps with 5-DOF force/torque sensing capability [72]. Two compact 3-DOF capacitive force sensors are integrated into the proximal regions of the forceps' two jaws to measure the grasping force and 3-DOF manipulation force, resulting in a 5-DOF force/torque. Additionally, a novel surgical palpation probe was proposed [73] as depicted in Figure 4d. Based on the capacitive sensing principle, this probe achieves six-axis force measurement and is ultimately applied to in vivo tissue detection.

MEMS force and tactile sensors perform exceptionally well in applications for robotic dexterous hands. Ge et al. proposed a capacitive sensor that combines proximity and pressure sensing [74], achieving both object proximity detection and contact force detection (up to 12 N), which is used for accurate grasping control in prosthetic hands (Figure 4e). As shown in Figure 4f, Muroyama et al. proposed a real-time force/temperature sensing system based on MEMS-LSI integration [75]. This system uses a capacitive sensor array to achieve simultaneous 3D force and temperature sensing, reducing the average force-sensing error from -0.98% to 0.072%. This ultimately enables precise grasping by a robotic arm. When it comes to electromagnetic sensing applications, Gong et al. proposed a flexible biomimetic triaxial tactile sensor based on a solid-liquid composite structure as

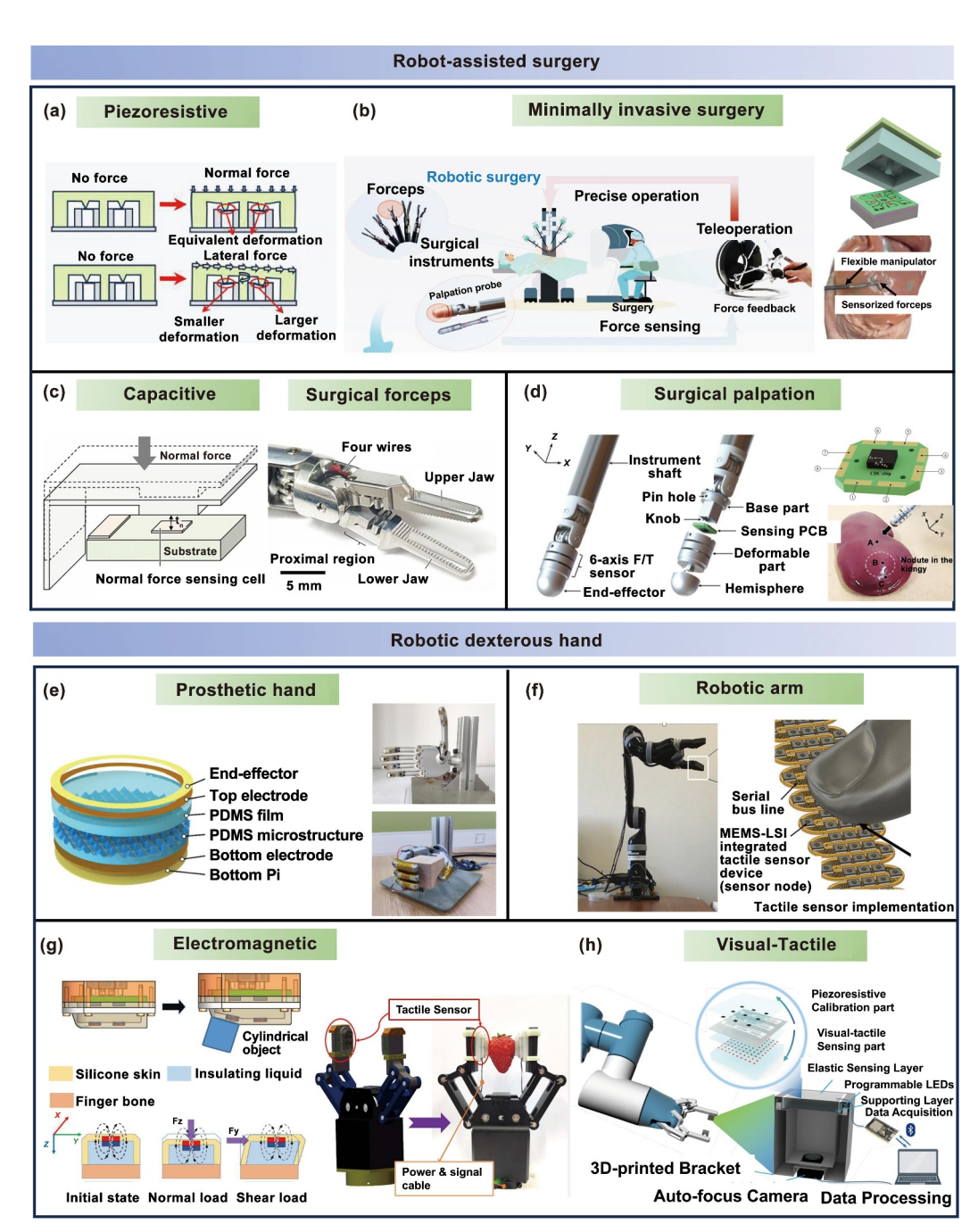


FIGURE 4 | MEMS force and tactile sensors. (a) Principle of piezoresistive MEMS force sensor. Reproduced from ref. [70]. Copyright 2025 Springer Nature. (b) Highly integrated 3D MEMS force sensing module. Reproduced from [24]. Copyright 2023 Wiley-VCH GmbH. Reproduced from ref. [71]. Copyright 2024 Springer Nature. (c) Application of capacitive sensor in surgical forceps. Reproduced from ref. [72]. Copyright 2018 IEEE. (d) Application of capacitive sensor in surgical palpation. Reproduced from ref. [73]. Copyright 2018 IEEE. (e) Application of capacitive sensor in prosthetic hand. Reproduced from ref. [74]. Copyright 2022 American Chemical Society. (f) Application of capacitive sensor in robotic arm. Reproduced from ref. [75]. CC BY 4.0. (g) Application of electromagnetic sensor in robotic arm. Reproduced from ref. [68]. Copyright 2024 IEEE. (h) Visual-tactile sensor. Reproduced from ref. [69]. Copyright 2024 IEEE.

shown in Figure 4g [68]. This sensor uses a magnetic field detection principle to achieve high-precision measurement of 3D contact forces. When an external force is applied to the flexible skin, it displaces a permanent magnet, causing a change in the magnetic field. A Hall sensor captures this magnetic signal, which is then mapped into 3D force data through a backpropagation (BP) neural network for decoupling. When integrated into a robotic gripper, this sensor enables object grasping. In addition, there are other types of MEMS tactile

sensors. As illustrated in Figure 4h, Hu et al. proposed a vision-tactile coupled sensor mechanism [69]. This sensor uses a piezoresistive unit to provide a baseline force signal, whereas optical markers generate a spatial weight based on displacement fields. The coupling of these two outputs a high-resolution force distribution, which significantly improves the accuracy and reliability of microforce measurements. This can be applied to human-robot interaction scenarios in fields such as robotic manipulation, wearable devices, and virtual reality.

Although MEMS force and tactile sensors offer high precision, miniaturization, and integration advantages, their rigid substrates and limited restrict their adaptability to large-area, deformable, or highly curved surfaces. These constraints have driven the development of flexible force and tactile sensors, which complement MEMS devices by providing conformal coverage and skin-like perception capabilities.

4.2 | Flexible Force And Tactile Sensors

Compared with MEMS sensors, flexible force and tactile sensors are fabricated using soft stretchable materials (e.g., polymers, elastomers, and conductive composites) and can conform to complex three-dimensional surfaces. Although MEMS devices excel in localized high-accuracy force/torque measurements and stable long-term performance, flexible sensors provide large-area coverage, multimodal sensing, and safer human interaction. In many robotic systems, these two types of sensors are complementary rather than mutually exclusive: MEMS sensors are often embedded at critical contact points for precise measurements, whereas flexible sensors form distributed arrays to deliver spatially rich tactile maps.

The core working principle of flexible force/tactile sensors can be summarized as the conversion of external mechanical stimuli, such as pressure, stretching, bending, and vibration, into measurable electrical signals, including changes in resistance, capacitance, voltage, or current. This process mimics the mechanoreceptors in human skin, which convert skin deformation into bioelectrical signals that are then transmitted to the brain via nerves. Flexible force and tactile sensors represent a pivotal branch of tactile sensing technology [76], characterized by their conformability, stretchability, and biomimetic design principles. Leveraging advanced functional materials and microstructure engineering, these sensors emulate the transduction mechanisms of biological skin to achieve distributed force mapping, texture discrimination, and environmental interaction capabilities. Based on the research of flexible force/tactile sensors, the concept of e-skin has been introduced. E-skin is a soft, stretchable, and ultrathin material that mimics the properties and functions of human skin [77]. It can detect various stimuli, such as pressure, temperature, humidity, and light, and respond to them in a manner similar to human skin. This makes it widely applicable in prosthetics, robotics, human-machine interfaces, virtual reality, health monitoring [78], and personalized medicine [79]. This section introduces common types of flexible tactile sensors/eskin and their applications in robotic sensing.

Common flexible tactile sensors include capacitive [80], triboelectric [81], piezoelectric [82], and resistive types [83]. Due to their unique sensing mechanisms and flexible compatibility, these technologies are profoundly transforming the environmental perception and interaction capabilities of robotic systems. One of the most widespread applications is tactile sensing. As shown in Figure 5a, Boutry et al. proposed a capacitive electronic skin with pyramidal microstructures [84]. Through a capacitive array design, it can measure and distinguish normal and tangential forces in real time. The pyramidal microstructures are distributed along nature-inspired phyllotaxis spirals, which significantly optimizes the sensor's sensitivity, hysteresis, and response time. Kong et al. proposed super-resolution tactile sensor arrays with sparsely distributed taxels powered by a universal intelligent framework (Figure 5b) [85]. Based on the resistive sensing principle, this sensor array can dynamically distinguish high-density pressure stimuli, enabling precise touch recognition.

Zhu's team has conducted in-depth research on thermoelectric sensing. As shown in Figure 5c, the team proposed a quadruple tactile sensor integrated into a robotic hand [86]. This sensor uses cross-coupled thermistors to simultaneously and independently sense multiple stimuli, including object material, contact pressure, object temperature, and ambient temperature. When combined with machine learning, the robotic hand can achieve high-precision waste sorting. Additionally, the team also proposed a flexible 6-DOF force/torque sensor with a simple structure, small size, and light weight [93]. This sensor uses stacked thin-film thermistors to sense the spatial strain of a flexible piezo-thermic material, achieving wide-range high-precision flexible sensing of 6-DOF force/torque. The team integrated the sensor into the fingertips of a robot's dexterous hand to enable delicate manipulation of objects. The working principle of iontronic sensor is based on the ion-electron interface effect. Its internal ionic electrolyte deforms under pressure, leading to a significant change in the electrical double-layer capacitance at the electrode interface, thereby achieving high-sensitivity detection of tiny pressures. As shown in Figure 5d, Bai et al. proposed a high-performance iontronic slip sensor [92]. By responding to both static pressure and dynamic vibrations through changes in capacitance, it achieves ultrahigh sensitivity and a fast responserelaxation time. Applied in robotic prostheses and tactile virtual reality, this sensor achieves high-precision texture recognition through a real-time visual interface, providing a new dimension for enhanced human-machine interaction.

In recent years, triboelectric flexible tactile sensors have achieved significant research breakthroughs in robotic applications. Lee's team designed an electronic skin that integrates two tactile sensors: a transient voltage artificial neuron (TVAN) and a sustained potential artificial neuron (SPAN) [87] as shown in Figure 5e. Featuring self-generated zero-biased signals, this system can perceive an object's complete information through a simple touch. The team also proposed a triboelectric multimodal tactile sensor with a multilayer structure [81], which was attached to a robot fingertip and analyzed using deep learning. The structure uses a differential contact area between two PTFE films to generate a voltage signal, enabling curvature measurement. By arranging a sensor array on the robot's finger, it can perceive the entire object. Liu's team proposed a stretchable electronic armor (E-armor) with a 3D crosslinked structure for colonoscopic continuum robots [88]. This system combines triboelectric encoding intelligence with an innovative stretchable triboelectric interlinked film (TIF) to form a triboelectric artificial synapse (Figure 5f). This enables autonomous adjustment of the continuum robot's posture while ensuring smooth operation.

In addition to the above types, there are other tactile sensors that can achieve excellent performance in specific applications. For example, as shown in Figure 5g, Dai et al. proposed an optical/electronic artificial skin that integrates optical fibers into

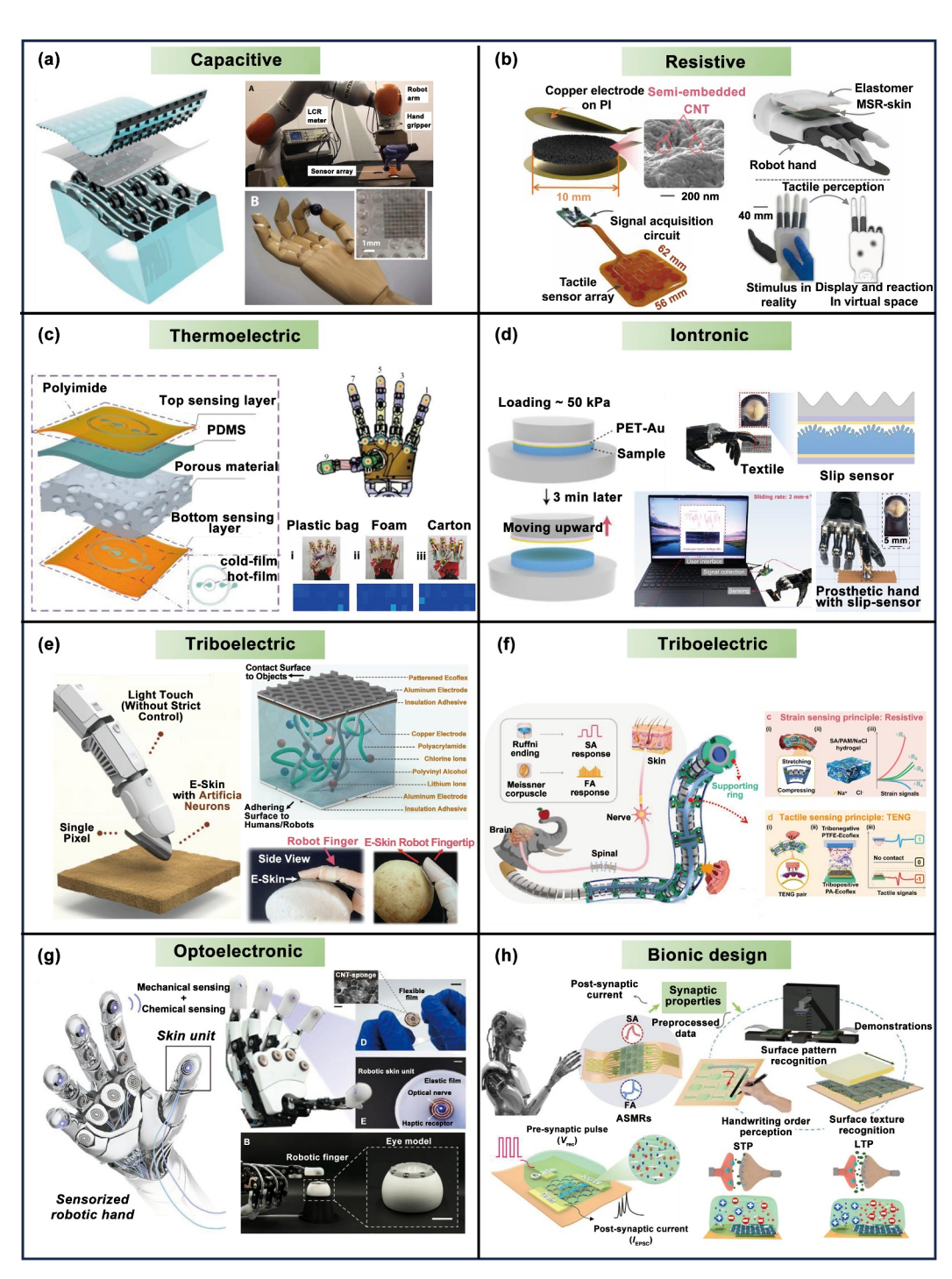


FIGURE 5 | Flexible force and tactile sensors. (a) Capacitive tactile sensor. Reproduced from ref. [84]. Copyright 2018 The American Association for the Advancement of Science. (b) Resistive super-resolution tactile sensor array. Reproduced from ref. [85]. Copyright 2025 The American Association for the Advancement of Science. (c) Thermoelectric quadruple tactile sensor. Reproduced from ref. [86]. Copyright 2020 The American Association for the Advancement of Science. (d) Iontronic slip sensor. Reproduced from ref. [92]. Copyright 2023 Springer Nature. (e) Triboelectric E-skin applied in robotic finger. Reproduced from ref. [87]. Copyright 2024 Wiley-VCH GmbH. (f) Triboelectric E-armor applied in colonoscopic continuum robot. Reproduced from ref. [88]. Copyright 2025 Wiley-VCH GmbH. (g) An optical/electronic artificial skin. Reproduced from ref. [89]. Copyright 2025 Springer Nature. (h) A bioinspired artificial mechanoreceptor array. Reproduced from ref. [90]. Copyright 2025 Springer Nature.

carbon nanotubes [89]. This allows the skin to sense force and temperature while also detecting near-infrared optical signals from molecules, providing a dual mode of physical and chemical sensing. When this sensor is integrated into a robotic arm, the robot can grade fruits based on their ripeness, hardness, and

sugar content. Furthermore, bioinspired designs have also recently attracted the attention of researchers [91]. As shown in Figure 5h, Hong et al. proposed a bioinspired artificial mechanoreceptor array that vertically integrates synaptic transistors with reduced graphene oxide channels to form artificial synaptic

mechanoreceptors with built-in synaptic functions [90]. Using machine learning, it performs surface pattern and texture recognition with fused slow- and fast-adapting postsynaptic values, offering high data efficiency and the potential for intelligent skin.

Flexible tactile sensing technology has progressed from detecting single physical quantities to a new stage of multidimensional perception and intelligent fusion. Through multimodal sensing mechanisms, biomimetic structural designs, and information fusion strategies, researchers have successfully achieved comprehensive perception of curvature, material, temperature, and even chemical signals, greatly enhancing a robot's ability to interact with the environment and make decisions in complex scenarios. These developments provide crucial technical support for the next generation of intelligent robots in industrial automation, domestic services, agricultural monitoring, and extreme-environment operations.

5 | Auditory Perception

Beyond physical contact and self-motion, a robot's ability to perceive and interact with its environment is profoundly enhanced by auditory perception. The sense of hearing enables critical functionalities for embodied AI, from understanding human voice commands in collaborative settings to detecting subtle acoustic signatures of impending mechanical failure or locating survivors in search-and-rescue missions. Based on the comparative data in Table 3, MEMS acoustic devices demonstrate significant advantages in miniaturization and high performance. MEMS microphones, with their chip-scale packaging, achieve extreme miniaturization while covering the core frequency range of human speech. They can capture environmental sounds with high fidelity, serving as a robot's "ears" for command reception, sound source localization, and industrial condition monitoring. Conversely, MEMS microspeakers also overcome size limitations, capable of outputting high sound pressure levels of up to 114 dB from a tiny footprint. Full-range models (500-10000 Hz) combine a low distortion rate of less than 1%, whereas low-frequency models complement this by enhancing bass performance. When used together, these two types of devices provide high-fidelity, immersive voice feedback and audio output for robots.

Due to their small size, high loudness, low distortion, and wide frequency response, MEMS microphones and microspeakers collectively form the core foundation for embodied AI robots to achieve natural and precise two-way voice interaction. This provides critical support for their environmental perception and humanized interaction capabilities. This section reviews key advancements in MEMS acoustic transducers, exploring their design principles and transformative applications in robotics.

5.1 | MEMS Microphones

MEMS microphones can be categorized into capacitive, piezoelectric, and piezoresistive types based on their transduction mechanisms. Among these, capacitive MEMS microphones forms the basis for many commercial microphones due to its CMOS compatibility, high sensitivity, and scalability [98]. Capacitive MEMS microphones typically consist of a diaphragm suspended above a fixed electrode, with an air gap enabling pressure-induced deflection. As shown in Figure 6a, this structural design allows sound waves to modulate capacitance, which is then translated into an electrical signal. The illustrated crosssection includes perforated backplate openings to reduce squeeze-film damping, whereas the fabricated prototype demonstrates millimeter-scale integration suitable for dense array deployment. Despite their wide adoption, these capacitive MEMS microphones face inherent limitations, including the requirement for a DC bias voltage to maintain transduction sensitivity and susceptibility to squeeze-film damping effects that restrict high-frequency response, which motivate ongoing innovations in advanced packaging strategies to mitigate these constraints.

Correspondingly, a representative structure of a MEMS microphone with chip-scale packaging is illustrated [29]. In Figure 6b, the microphone comprises a MEMS diaphragm, an application-specific integrated circuit (ASIC), and an acoustic chamber integrated within a ceramic substrate. Sound enters through perforated openings and travels into a Helmholtz chamber, where it excites the diaphragm. The diaphragm's vibration alters the electrical characteristics of the sensing element, which are then processed by the ASIC. This compact integrated design significantly minimizes the front volume, suppresses undesirable acoustic resonances, and ensures a linear frequency response over a wide range. These advantages make it suitable for robotic auditory assistance systems to perform environmental perception.

Beyond conventional auditory functions, MEMS microphones have emerged as critical diagnostic tools in industrial robotics, enabling noncontact monitoring of mechanical systems through acoustic signature analysis. An industrial application of MEMS microphones in condition-based maintenance systems is shown in Figure 6c. In this setup, an omnidirectional capacitive

 TABLE 3
 Comparison of microphones and microspeakers.

Ref.	Device type	Dimension	SPL	Frequency range	THD (%)
[29]	Microphone	2.05 × 2.8 mm	N/A	100-10000 Hz	N/A
[94]	Microphone	N/A	N/A	10-15000 Hz	N/A
[95]	Microphone	$32 \times 21 \text{ mm}$	90 dB	1000-20000 Hz	1.41
[96]	Microphone	$30 \times 30 \text{ mm}$	114 dB	100-2500 Hz	N/A
[30]	Microspeaker	$4.5 \times 4.5 \text{ mm}$	> 107 dB	500-10000 Hz	< 1
[97]	Microspeaker	$20 \times 13 \text{ mm}$	98.4 dB	20-1000 Hz	N/A

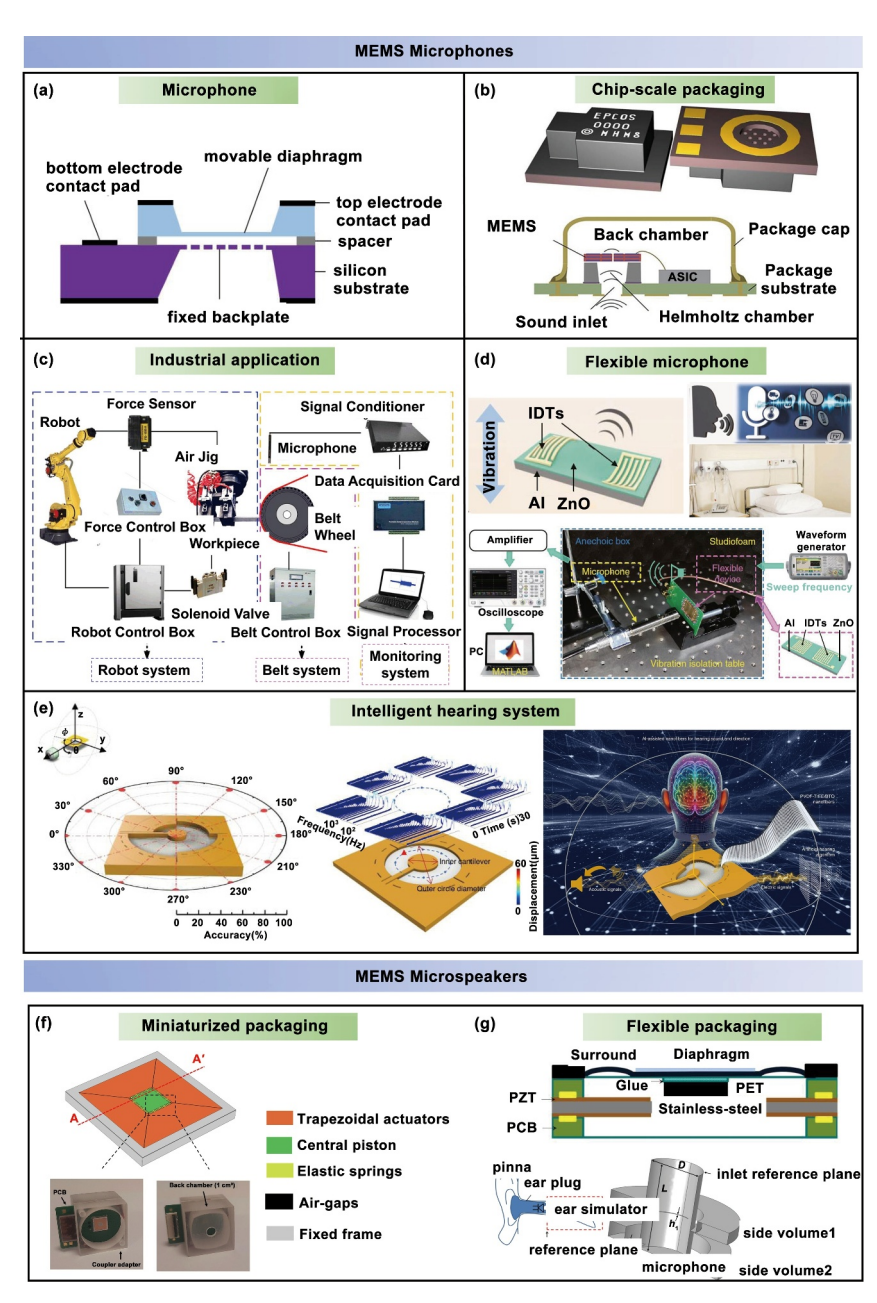


FIGURE 6 | Representative MEMS microphones and microspeakers. (a) A cross-sectional structure of a MEMS capacitive microphone showing diaphragm deflection and air-gap modulation. Reproduced from ref. [99]. Copyright 2020 MDPI. (b) A MEMS microphone with chip-scale packaging integrating a Helmholtz chamber and ASIC for improved frequency response. Reproduced from ref. [29]. Copyright 2010 Springer Nature. (c) Robotic grinding system using a MEMS microphone for acoustic-based belt condition monitoring via machine learning. Reproduced from ref. [94]. Copyright 2018 Elsevier Ltd. (d) A flexible piezoelectric MEMS microphone based on ZnO thin film, capable of both sound sensing and speech recognition. Reproduced from ref. [95]. Copyright 2019 Hindawi and 2022 Springer Nature. (e) Piezoelectric nanofiber-based intelligent hearing system. Reproduced from ref. [96]. CC BY 4.0. (f) Full-range MEMS piezoelectric microspeaker with folded spring-actuated diaphragm structure for in-ear applications. Reproduced from ref. [30]. Copyright 2023 IEEE. (g) MEMS piezoelectric microspeakers with flexible packaging. Reproduced from ref. [97]. Copyright 2025 MDPI.

microphone is embedded in a robotic grinding platform to capture acoustic signals related to abrasive belt wear [94]. This application exemplifies a powerful paradigm for robotic self-awareness: using onboard microphones to perform acoustic-based condition monitoring. By learning the sound of normal operation, a robot can predictively diagnose its own or its tools' health, enabling predictive maintenance and reducing operational downtime.

Based on the evolving demands for bioinspired robotic perception, the emergence of flexible piezoelectric MEMS microphones represents a transformative approach to overcoming the form-factor limitations of conventional acoustic sensors in deformable robotic systems. A flexible piezoelectric microphone design capable of bidirectional operation is demonstrated in Figure 6d. This structure supports high-fidelity speech recognition with over 98% accuracy and offers good mechanical

flexibility, making it ideal for integration into soft robots [95]. In the future, the developmental potential of MEMS microphones lies in the creation of intelligent robotic auditory systems, which will enable embodied intelligent robots to better communicate with humans. For example, Chang et al. developed an intelligent hearing system inspired by the human auditory system [96] as shown in Figure 6e. This system mimics the cochlear structure, using piezoelectric nanofibers to transmit and convert sound signals into electromechanical signals. This intelligent auditory system surpasses human auditory directional capabilities, demonstrating the excellent interactive performance of future MEMS microphones.

5.2 | MEMS Microspeakers

Although MEMS microphones provide robots with the ability to hear. MEMS microspeakers enable them to speak. To achieve full-range output in compact acoustic systems, a MEMS microspeaker with a piston-type actuator has been developed. As illustrated in Figure 6f, the speaker employs four trapezoidal piezoelectric plates connected via folded parylene springs to drive a central diaphragm. This structure enhances lowfrequency displacement while preventing acoustic leakage between chambers. Its minimal packaging and broadband performance make it a strong candidate for next-generation in-ear audio solutions [30]. Shih et al. proposed two structures of piezo-actuated microspeakers fabricated using the aerosol deposition method and metal microfabrication in Figure 6g [97]. These microspeakers exhibit flexibility greater than 10 mm·N⁻¹ at their edges, demonstrating good flexibility while significantly enhancing their sound pressure level performance in the lowfrequency range. For robots, microspeakers mean they can emit clearer, more directional audio cues or warnings, or simulate more natural vocalizations during human-robot interaction.

6 | Olfactory Perception

Although sight, hearing, and touch replicate and enhance human-like perception, olfactory perception, or machine olfaction represents a new robotic sensing modality that can endow robots with capabilities far beyond human limits, enabling robots to distinguish common odors/gases, detect specific gas concentrations, and dynamically localize odor/gas sources. Compared with traditional passive gas sensing systems, this technology significantly enhances environmental comprehension of robot through its capacity to perceive, track, and precisely characterize gas concentrations, types, and spatial distributions. The ability to "smell" allows a robot to detect hazardous chemical leaks, identify explosives, or even diagnose diseases from volatile organic compounds (VOCs)—tasks that are either dangerous or impossible for humans. This noncontact chemical sensing modality is critical for robot applications in environmental monitoring, disaster response, and industrial safety. The core of a robotic olfactory system comprises two key components: gas sensor that act as the artificial nose and algorithms for gas recognition and source localization. Gas sensors obtain environmental chemical information,

recognition and localization algorithms analyze gas types/concentrations and infer source positions. This section explores the key technologies and challenges in building these "electronic noses" for embodied agents.

6.1 | Gas Sensors

Gas sensors serve as the hardware base of robotic olfactory systems, converting molecular interactions with sensing materials into processable electrical signals. Multiple types of gas sensors have been developed [100, 101], as shown in Figure 7a, primarily categorized into semiconductor [102], catalytic combustion [103], electrochemical [104], and optical sensors [105] based on their distinct operating principles, among others. Semiconductor gas sensors utilize the conductivity changes of metal oxide materials upon gas exposure, offering advantages in cost-efficiency, high sensitivity, and rapid response. Catalytic combustion sensors detect flammable gases via temperature changes induced by catalytic oxidation, providing accurate quantification and fast response. Optical gas sensors detect gas concentrations by exploiting either the inherent optical properties of target gases or gas-induced alterations in the optical characteristics of sensing materials. Spectral absorption-based sensors, that is, infrared gas sensors, dominate this category. Electrochemical gas sensors detect gases by measuring current variations generated during redox reactions in an electrolyte, offering advantages such as linear output characteristics and low power consumption. However, cross-sensitivity among coexisting gases with similar structures and properties remains a critical challenge, leading to detection inaccuracies that hinder practical olfactory applications in robots.

We compared two commercial CH₄ sensors. The MEMS CH₄ sensor achieved a resolution of 3% F.S. with a volume of $4 \times 4 \times 1$ mm, whereas the electrochemical CH₄ sensor achieved a resolution of 2% F.S. with a volume of 20 \times 20 \times 16 mm. With a comparable resolution, the MEMS sensor achieved a significantly smaller volume and lower power consumption. Therefore, MEMS technology has led to significant improvements in the size and performance of gas sensors. For instance, MEMS enables the fabrication of microheaters on silicon substrates, drastically reducing the power consumption of metaloxide semiconductor (MOS) sensors, which traditionally require high operating temperatures. MEMS processes are also used to create microscale electrochemical cells and miniaturized optical cavities for spectroscopic sensors. This miniaturization is not just about size reduction and it is the key to creating lowcost, low-power, and high-density gas sensors.

6.2 | Gas Recognition and Mixed Gas Detection

Gas sensor array technology, commonly termed "electronic nose", employs multiple sensors to obtain multidimensional gas features, which are subsequently processed by pattern recognition algorithms for gas identification. As shown in Figure 7bi, Persaud et al. pioneered the first gas sensor array [106], which can distinguish diverse odors consistently, using multiple semiconductor gas sensors, demonstrating that odor

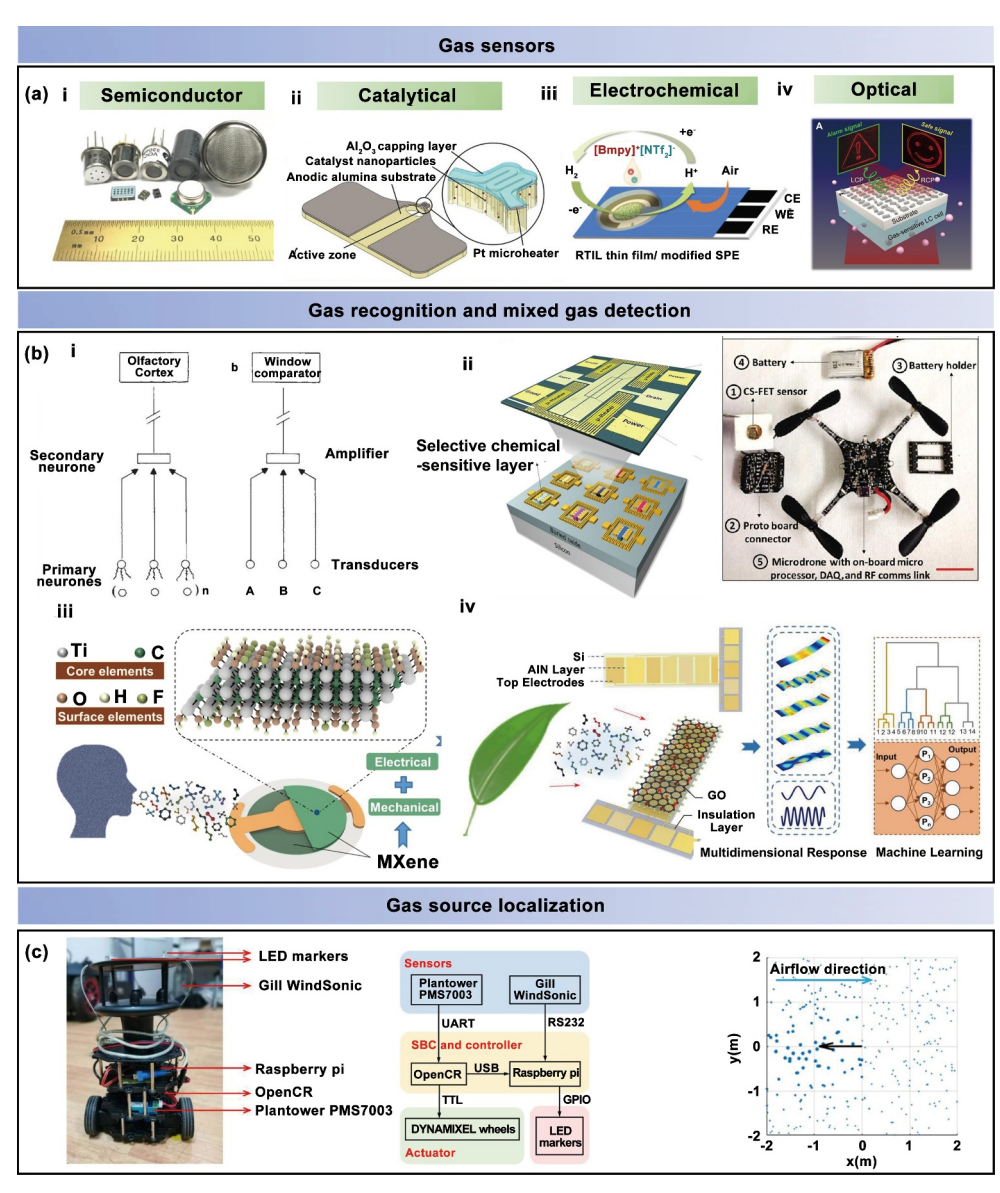


FIGURE 7 | Schematic diagram of the MEMS olfactory sensor: (a) Various types of gas sensors: (i) Semiconductor sensor. Reproduced from ref. [102]. Copyright 2020 Springer Nature. (ii) Catalytic sensor. Reproduced from ref. [103]. Copyright 2024 Elsevier Ltd. (iii) Electrochemical sensor. Reproduced from ref. [104]. Copyright 2024 American Chemical Society. (iv) Optical sensor. Reproduced from ref. [105]. CC BY 4.0. (b) Gas recognition and mixed gas detection: (i) Electronic nose. Reproduced from ref. [106]. Copyright 1982 Springer Nature. (ii) Chemosensitive field-effect transistor array. Reproduced from ref. [28]. CC BY 4.0. (iii) Piezoelectric virtual sensor array. Reproduced from ref. [110]. Copyright 2021 American Chemical Society. (iv) Miniaturization of virtual sensor array. Reproduced from ref. [107]. Copyright 2022 American Chemical Society. (c) Gas source localization algorithms. Reproduced from ref. [108]. Copyright 2020 Elsevier Ltd.

discrimination can be reliably achieved without specific sensing materials. Fahad et al. developed a 3.5 nm silicon channel transistor-based chemo-sensitive field-effect transistor array [28], achieving high selectivity and low limit of detection (1 ppb) for multigas detection at room temperature, as illustrated in Figure 7bii. To address limitations in size, energy consumption, and reliability of physical sensor arrays, virtual sensor arrays have emerged as a research focus for gas sensors [111]. Li et al. proposed a piezoelectric virtual sensor array (VSA) using quartz crystal microbalance sensors based on Butterworth–Van Dyke equivalent models [110]. By extracting multiple characteristics from sensing films and employing support vector machines and artificial neural networks (ANNs), the VSA successfully identified gases with similar structure with an accuracy of 90%

(Figure 7biii). To further advance miniaturization of virtual sensor array, Li et al. employed multimodal frequency shifts in piezoelectric resonant cantilevers as sensing responses to VOCs [107] as depicted in Figure 7biv. Based on ANN algorithms, the proposed VSA achieved precise discrimination of individual VOCs and their mixtures with accuracies of 95.8% and 87.5%.

6.3 | Gas Source Localization

Gas source localization algorithms represent a pivotal technology in robotic olfaction, enabling robots to identify and pinpoint emission sources through sensor-derived concentration data.

This process typically involves three subtasks: (1) gas search (detecting environmental presence), (2) gas tracking (following plume trajectories), and (3) source verification (precisely determining source positions through sensor data integration). Research in robotic odor localization began in the 1990s. Ishida et al. developed biomimetic strategies including moth-inspired search, gradient-based tracking, and upwind navigation [112]. Haves et al. demonstrated enhanced localization efficiency through swarm robotics using Moorebots platforms with collective communication [109]. Chen et al. developed multiple smoke source localization algorithms by optimizing multimodal probability maps [108], achieving high-precision source localization. For smoke plume tracking in unknown environments, a local perception window particle filtering approach was employed, as shown in Figure 7c, with enhanced localization success rates attained through integration of a modified firefly algorithm. The average computation time including plume path estimation, resampling, and target evaluation in every step is 35.9974 ms and the average smoke source localization error is 0.7769 m. In complex obstacle-laden settings, the incorporation of deep Qnetwork algorithms ensured collision-free robotic navigation while maintaining precise smoke source identification.

6.4 | Application

Although significant progress has been made, the deployment of robust olfactory robots outside the laboratory faces hurdles, such as sensor drift, real-world environmental dynamics, and the sheer complexity of chemical landscapes. Future breakthroughs will likely emerge from the convergence of several fields, such as AI-driven sensor design and materials discovery. Instead of relying on trial-and-error, machine learning will be used to predict and design new sensing materials with targeted affinities and sensitivities. AI will also enable self-calibrating sensors that can adapt to drift and environmental changes over time. The ultimate goal is to mimic the staggering efficiency and sensitivity of biological olfaction. This involves developing neuromorphic olfactory chips that process signals in an event-driven manner as well as exploring bio-hybrid systems that integrate living olfactory cells or receptors directly with electronic interfaces. The future of environmental monitoring lies in deploying swarms of small low-cost olfactory robots. These swarms can collaboratively map a chemical plume in 3D, locate its source with unprecedented speed and accuracy, and create a dynamic distributed sensory network. In conclusion, machine olfaction is arguably one of the most challenging yet rewarding frontiers for embodied AI. Overcoming its challenges will not only create powerful new tools for industry and safety but also push the very boundaries of what we consider "robotic perception".

7 | Conclusion and Outlook

This review has systematically charted the critical role of MEMS as the burgeoning sensory nervous system for embodied AI robots. From mapping the external world with ranging sensors to achieving self-awareness through inertial sensors, and from discerning physical interactions via force and tactile sensing to

perceiving the environment through auditory and olfactory modalities, a clear narrative emerges: MEMS technology is the fundamental enabler for the rich multimodal perception demanded by next-generation robots. Its intrinsic scalability, performance, and miniaturization are breaking down the long-standing barriers to creating truly autonomous agents that can perceive, reason, and act in the complex physical world.

The rise of MEMS sensors as a cornerstone for embodied AI applications is not by chance; their intrinsic properties perfectly complement the core requirements of embodied AI robots. MEMS technology can fabricate complex mechanical and electronic structures on millimeter- or even micrometer-scale chips [25, 93], achieving exceptionally high spatial efficiency. For a robot to achieve human-like or animal-like dexterity, its sensors must be seamlessly integrated into confined spaces, such as joints and fingertips, without compromising its range of motion or appearance. MEMS accelerometers, gyroscopes, and force sensors can fulfill this requirement. Furthermore, MEMS technology allows for the large-scale deployment of miniaturized sensors throughout a robot's body, forming a "sensing network" that provides rich multidimensional environmental interaction data to AI models [113], which is a prerequisite for achieving true "embodied" perception. Meanwhile, MEMS sensors maintain excellent sensitivity while ensuring high integration, making them more suitable for embodied AI robot applications compared to traditional sensors.

7.1 | Challenges and Opportunities

Although MEMS technology has made significant strides in the field of robotic sensing and actuation, several major challenges must be overcome to fully unlock the potential of autonomous embodied AI systems. When it comes to manufacturing processes and mass production, a significant challenge lies in the diverse fabrication techniques required for different categories of MEMS sensors [114]. This heterogeneity makes it difficult to establish a single standardized manufacturing platform. As a result, the mass production of multiple sensor types on a single production line is not feasible, hindering their large-scale lowcost implementation in multifunctional integrated robots. Regarding system integration, mechanically integrating MEMS sensors with robots poses considerable difficulty [115]. In spatially constrained areas, such as robotic joints and endeffecters, it is challenging to ensure both high-precision stable mounting and to prevent measurement errors caused by mechanical stress, vibration, or thermal deformation. Additionally, the optimal mounting positions for different sensors often conflict, wiring is complex, and the dynamic coupling effects between the sensors and the robot's structure must be considered, which further increases the complexity of mechanical integration.

Emerging trends are creating vast opportunities for the next generation of robotic MEMS technology. The rise of edge computing enables MEMS sensors to process data locally on the robot [116, 117], significantly reducing latency and enhancing real-time control capabilities. This is particularly critical for autonomous decision-making in dynamic environments. The

integration of advanced materials, such as two-dimensional materials, such as graphene [118–120], is expected to lead to the development of ultrasensitive sensors. Furthermore, multisensor fusion is becoming a key enabler for robust perception. By intelligently combining data from diverse MEMS sensors (such as IMUs, ToF, and capacitive proximity sensors), robots can achieve more accurate and reliable environmental understanding, overcoming the limitations of any single sensing modality. Together, these innovations form the foundation for MEMS technology to advance toward higher performance and broader applications in the field of embodied AI robotics.

7.2 | Sensory Nervous System of Robots

Conceptualizing MEMS as an integrated "sensory nervous system" is a biomimetic framework to understand the field's evolution from discrete components to intelligently interconnected architectures. Each MEMS sensor, such as an accelerometer, gyroscope, magnetometer, or pressure sensor, can be viewed as a specialized neuron that transduces a specific physical stimulus (motion, angular rate, magnetic field, or pressure) into a digital electrical signal. This fundamental transduction process is analogous to how biological receptors convert external stimuli into neural impulses [121]. The limitations of individual MEMS "neurons" are evident as their performance can degrade over time or in specific environments.

The integrated nervous system architecture is realized when these disparate signals are intelligently combined through sensor fusion. This process acts like the brain's analytical center, leveraging the strengths of one sensor to compensate for the weaknesses of another. For example, the long-term low-frequency stability of an accelerometer can be used to correct the high-frequency drift output of a gyroscope. The absolute heading data from a magnetometer can then be used to compensate for gyroscopic drift and provide a global directional reference. Combining the three axes of acceleration, angular velocity, and magnetic field data in a 9-axis IMU creates a system that is more accurate, reliable, and robust than any single sensor alone. This represents a critical shift from simply collecting data points to generating actionable, intelligent insights, realizing the biomimetic vision of a comprehensive sensory nervous system.

Integrating diverse sensor outputs into a unified and reliable data stream is the central challenge and defining characteristic of an effective MEMS "sensory nervous system" as shown in Figure 8. Cross-modal data fusion is a computational process that overcomes the inherent limitations of individual sensors, such as noise, drift, and environmental sensitivity, to produce a single optimal output. This process is fundamental to creating robust and accurate systems for applications such as autonomous navigation, robotics, and consumer electronics. The methods for achieving this fusion range from simple low-cost algorithms, such as complementary filters and Kalman filters, to highly complex computationally intensive models, each with its unique trade-offs and application-specific advantages. In

recent years, emerging algorithms, such as deep learning, have begun to gain prominence [122, 123], offering new research avenues for multimodal data fusion.

7.3 | Outlook

Looking forward, the trajectory of MEMS sensing for robotics is poised for a revolutionary leap, driven by deep integration at both the hardware and software levels. Instead of merely improving individual sensor metrics, the future lies in creating synergistic systems where perception and cognition are intrinsically linked. We foresee some pivotal frontiers shaping the next era of robotic intelligence.

At the hardware level, the convergence of MEMS and in-sensor computing promises to redefine the very nature of sensory data [124-126]. The imminent 3D integration of MEMS sensor arrays with nonvolatile memory technologies, such as memristors, will shift computation from the cloud or central processor directly into the sensor itself. This paradigm shift will transform sensors from passive data collectors into active interpreters. For instance, a robotic fingertip equipped with such a device would no longer stream raw pressure data. Instead, it could directly output semantic information such as "object slipping," "texture recognized as fabric," or "sharp edge detected." This on-chip near-zero-latency processing will be critical for robots requiring instantaneous reflexes, such as in highspeed manufacturing or delicate surgical procedures, fundamentally enabling a new class of safe and responsive physical interactions.

At the application level, the rich multimodal data streams from integrated MEMS "multi-sense" platforms will unlock the full potential of large language and multimodal models (LLMs/ LMMs) in the physical world [127, 128]. Although current LLMs excel in the digital domain, their interaction with reality is limited. A robot equipped with a full suite of MEMS sensors feeling the subtle vibrations of a motor (IMU), touching the texture of an object (tactile skin), seeing its shape (LiDAR), hearing a user's command (microphone), and even smelling a potential gas leak (olfactory sensor)—can provide the rich, grounded, and real-time context that LLMs desperately need. This fusion will spawn novel applications previously confined to science fiction. Imagine a home-assistant robot that not only understands the command "check if the stove is on" but also can physically go, feel for residual heat, "smell" for gas, and provide a multisensory-verified definitive answer. Or a searchand-rescue robot that can navigate rubble, identify a survivor by faint sounds and body heat and communicate its findings in natural language. The integration of comprehensive MEMS sensing with powerful AI models will be the catalyst that finally allows robots to move beyond executing preprogrammed tasks and begin to truly understand, reason about, and interact with the unstructured physical world.

In essence, the future of embodied AI will be built upon this powerful symbiosis: MEMS providing the rich, semantic-aware

MEMS Sensing System for Embodied AI Robots

Information processing

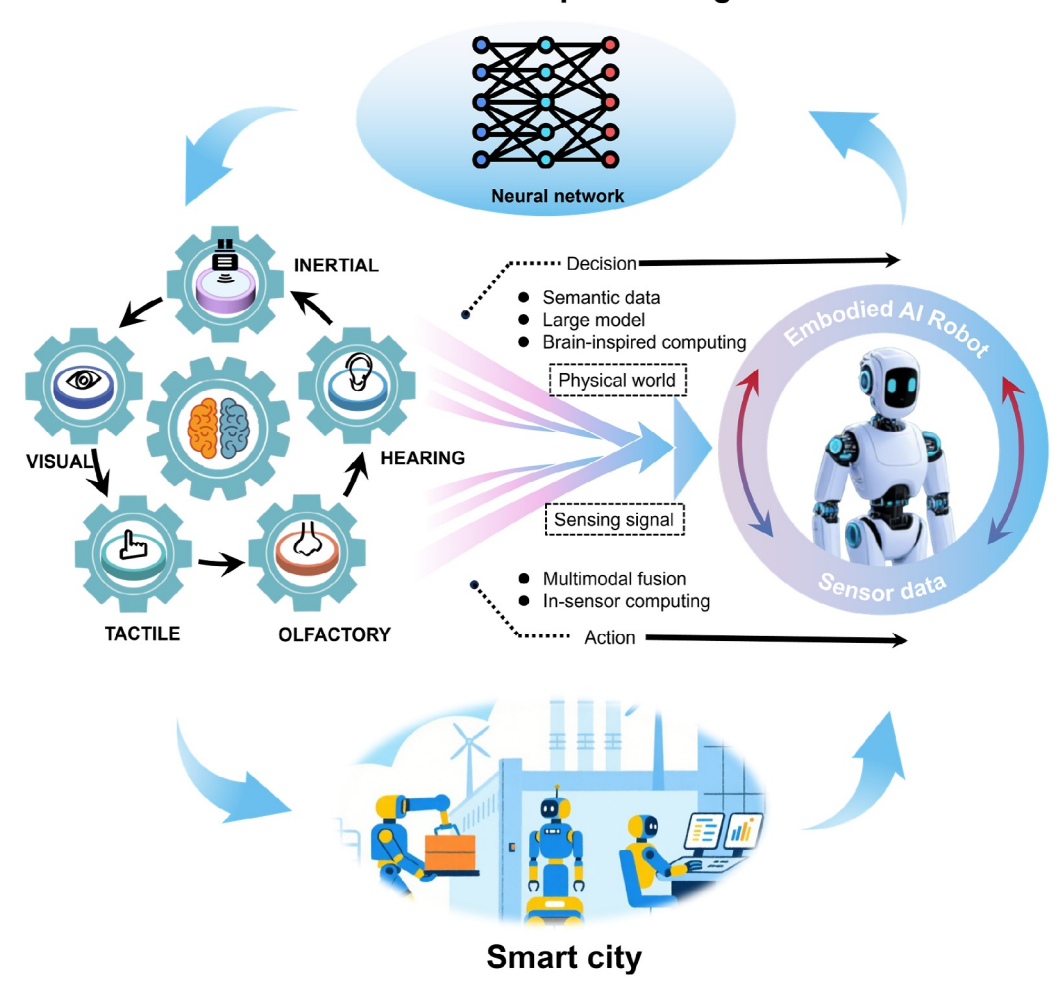


FIGURE 8 | Outlook of MEMS sensors for embodied AI robots.

"sensory neurons" and large models providing the "cognitive brain". This combination will not just make robots more capable but will usher in an era of truly perceptive and intelligent machines.

Author Contributions

Xu Zhou: writing – original draft, visualization. Dongsheng Li: writing – original draft, visualization. Shuhan He: writing – original draft, visualization. Mengyao Xiao: writing – original draft, visualization. Zhouli Sui: writing – original draft, visualization. Fusheng Zha: methodology, validation. Lining Sun: methodology, supervision, resources, project administration, writing – review and editing. Chengkuo Lee: investigation, visualization, writing – review and editing, methodology. Huicong Liu: conceptualization, writing – review and editing, funding acquisition, writing – original draft, methodology.

Acknowledgments

The authors acknowledge financial support from the following research grants: Natural Science Foundation of Jiangsu Province for Distinguished Young Scholars (Grant No. BK20220056) and National Natural Science Foundation of China (Grant No. 52475599).

Conflicts of Interest

The authors declare no conflicts of interest.

References

- 1. J. Li, and S. X. Yang, "Digital Twins to Embodied Artificial Intelligence: Review and Perspective," *Intelligence & Robotics* 5, no. 1 (2025): 202–227, https://doi.org/10.20517/ir.2025.11.
- 2. Y. Fan, Z. Pei, C. Wang, M. Li, Z. Tang, and Q. Liu, "A Review of Quadruped Robots: Structure, Control, and Autonomous Motion," *Advanced Intelligent Systems* 6 (2024): 2300783, https://doi.org/10.1002/aisy.202300783.
- 3. J. Ni, Y. Chen, G. Tang, J. Shi, W. Cao, and P. Shi, "Deep Learning-Based Scene Understanding for Autonomous Robots: A Survey," *Intelligence & Robotics* 3 (2023): 374–401, http://dx.doi.org/10.20517/ir.2023.22.
- 4. Y. Hu, H. Su, J. Fu, et al., "Nonlinear Model Predictive Control for Mobile Medical Robot Using Neural Optimization," *IEEE Transactions on Industrial Electronics* 68, no. 12 (2021): 12636–12645, https://doi.org/10.1109/tie.2020.3044776.
- 5. A. Padmanabha, J. Gupta, C. Chen, et al., "Independence in the Home: A Wearable Interface for a Person with Quadriplegia to Teleoperate a Mobile Manipulator," in *Proceedings of the 2024 ACM/IEEE*

- International Conference on Human-Robot Interaction (2024), 542–551, https://doi.org/10.1145/3610977.3634964.
- 6. J. Wang, C. Yue, G. Wang, et al., "Task Autonomous Medical Robot for Both Incision Stapling and Staples Removal," *IEEE Robotics and Automation Letters* 7, no. 2 (2022): 3279–3285, https://doi.org/10.1109/lra.2022.3141452.
- 7. J. Wu, R. Antonova, A. Kan, et al., "Tidybot: Personalized Robot Assistance With Large Language Models," *Autonomous Robots* 47, no. 8 (2023): 1087–1102, https://doi.org/10.1007/s10514-023-10139-z.
- 8. K. Rao, X. Wei, S. Zhang, et al., "A MEMS Micro-g Capacitive Accelerometer Based on Through-Silicon-Wafer-Etching Process," *Micromachines* 10, no. 6 (2019): 380, https://doi.org/10.3390/mi10060380.
- 9. W. A. Gill, I. Howard, I. Mazhar, and K. McKee, "A Review of MEMS Vibrating Gyroscopes and Their Reliability Issues in Harsh Environments," *Sensors* 22, no. 19 (2022): 7405, https://doi.org/10.3390/s22197405.
- 10. C. Tu, X. H. Ou-Yang, Y. J. Wu, and X. S. Zhang, "Single-Structure 3-Axis Lorentz Force Magnetometer Based on an aln-on-si MEMS Resonator," *Microsystems & Nanoengineering* 10, no. 1 (2024): 58, https://doi.org/10.1038/s41378-024-00696-3.
- 11. C. Hou, K. Wang, F. Wang, et al., "A Highly Integrated 3D MEMS Force Sensing Module With Variable Sensitivity for Robotic-Assisted Minimally Invasive Surgery," *Advanced Functional Materials* 33, no. 43 (2023): 2302812, https://doi.org/10.1002/adfm.202302812.
- 12. C. Xu, Y. Wang, J. Zhang, et al., "Three-Dimensional Micro Strain Gauges as Flexible, Modular Tactile Sensors for Versatile Integration With Micro- and Macroelectronics," *Science Advances* 10, no. 34 (2024): eadp6094, https://doi.org/10.1126/sciadv.adp6094.
- 13. Z. Zhao, J. Tang, J. Yuan, et al., "Large-Scale Integrated Flexible Tactile Sensor Array for Sensitive Smart Robotic Touch," *ACS Nano* 16, no. 10 (2022): 16784–16795, https://doi.org/10.1021/acsnano.2c06432.
- 14. X. Yue, J. Wang, H. Yang, et al., "A Drosophila-Inspired Intelligent Olfactory Biomimetic Sensing System for Gas Recognition in Complex Environments," *Microsystems & Nanoengineering* 10, no. 1 (2024): 153, https://doi.org/10.1038/s41378-024-00752-y.
- 15. H. M. Fahad, H. Shiraki, M. Amani, et al., "Room Temperature Multiplexed Gas Sensing Using Chemical-Sensitive 3.5-nm-Thin Silicon Transistors," *Science Advances* 3 (2017): e1602557, https://doi.org/10.1126/sciadv.1602557.
- 16. M. Winter, G. Feiertag, A. Leidl, and H. Seidel, "Influence of a Chip Scale Package on the Frequency Response of a MEMS Microphone," *Microsystem Technologies* 16, no. 5 (2010): 809–815, https://doi.org/10.1007/s00542-009-0994-z.
- 17. C. Gazzola, V. Zega, F. Cerini, S. Adorno, and A. Corigliano, "On the Design and Modeling of a Full-Range Piezoelectric MEMS Loudspeaker for In-Ear Applications," *Journal of Microelectromechanical Systems* 32, no. 6 (2023): 626–637, https://doi.org/10.1109/jmems.2023. 3312254.
- 18. J. Huang, H. Wang, J.-a. Li, et al., "High-Performance Flexible Capacitive Proximity and Pressure Sensors With Spiral Electrodes for Continuous Human–Machine Interaction," *ACS Materials Letters* 4, no. 11 (2022): 2261–2272, https://doi.org/10.1021/acsmaterialslett.2c00860.
- 19. Q. Shi, Z. Sun, X. Le, J. Xie, and C. Lee, "Soft Robotic Perception System With Ultrasonic Auto-Positioning and Multimodal Sensory Intelligence," *ACS Nano* 17, no. 5 (2023): 4985–4998, https://doi.org/10.1021/acsnano.2c12592.
- 20. L. Mollard, J. Riu, S. Royo, et al., "Biaxial Piezoelectric MEMS Mirrors With Low Absorption Coating for 1550 Nm Long-Range LIDAR," *Micromachines* 14, no. 5 (2023): 1019, https://doi.org/10.3390/mi14051019.
- 21. Y. Bai, B. Zhang, N. Xu, J. Zhou, J. Shi, and Z. Diao, "Vision-Based Navigation and Guidance for Agricultural Autonomous Vehicles and

- Robots: A Review," *Computers and Electronics in Agriculture* 205 (2023): 107584, https://doi.org/10.1016/j.compag.2022.107584.
- 22. W. Chen, W. Chi, S. Ji, et al., "A Survey of Autonomous Robots and Multi-Robot Navigation: Perception, Planning and Collaboration," *Biomimetic Intelligence and Robotics* 5, no. 2 (2025): 100203, https://doi.org/10.1016/j.birob.2024.100203.
- 23. R. Singh and K. S. Nagla, "Comparative Analysis of Range Sensors for the Robust Autonomous Navigation—A Review," *Sensor Review* 40, no. 1 (2020): 17–41, https://doi.org/10.1108/sr-01-2019-0029.
- 24. Y. Al-Handarish, O. M. Omisore, T. Igbe, et al., "A Survey of Tactile-Sensing Systems and Their Applications in Biomedical Engineering," *Advances in Materials Science and Engineering* 2020, no. 1 (2020): 4047937, https://doi.org/10.1155/2020/4047937.
- 25. R. Peng, Y. Wang, M. Lu, and P. Lu, "A Dexterous and Compliant Aerial Continuum Manipulator for Cluttered and Constrained Environments," *Nature Communications* 16, no. 1 (2025): 889, https://doi.org/10.1038/s41467-024-55157-2.
- 26. K. Sugimoto and S. Nagasawa, "Micro-Hexapod Robot With an Origami-Like SU-8-Coated Rigid Frame," *Robotica* 42, no. 5 (2024): 1614–1627, https://doi.org/10.1017/s0263574724000419.
- 27. T. Thurner, T. Kammerhofer, B. Reiterer, and M. Hofbaur, "Tactile Sensor Solution With MEMS Pressure Sensors in Industrial Robotics," *Elektrotech. Inftech.* 140, (2023): 541–550, https://doi.org/10.1007/s00502-023-01159-9.
- 28. A. E. Valles, V. R. Alva, and I. Belokonov, "Calibration Method of MEMS Gyroscopes Using a Robot Manipulator," *IEEE Aerospace and Electronic Systems Magazine* 38, no. 3 (2023): 20–27, https://doi.org/10.1109/maes.2022.3232728.
- 29. D. Wang, H. Xie, L. Thomas, and S. J. Koppal, "A Miniature Lidar With a Detached MEMS Scanner for Micro-robotics," *IEEE Sensors Journal* 21, no. 19 (2021): 21941–21946, https://doi.org/10.1109/jsen. 2021.3079426.
- 30. Y. Xu, S. Zhang, S. Li, et al., "A Soft Magnetoelectric Finger for Robots' Multidirectional Tactile Perception in Non-Visual Recognition Environments," *NPJ Flexible Electronics* 8, no. 1 (2024): 2, https://doi.org/10.1038/s41528-023-00289-6.
- 31. D. Wang, C. Watkins, and H. Xie, "MEMS Mirrors for Lidar: A Review," *Micromachines* 11, no. 5 (2020): 456, https://doi.org/10.3390/mi11050456.
- 32. P. Trocha, M. Karpov, D. Ganin, et al., "Ultrafast Optical Ranging Using Microresonator Soliton Frequency Combs," *Science* 359, no. 6378 (2018): 887–891, https://doi.org/10.1126/science.aao3924.
- 33. X. Zhang, K. Kwon, J. Henriksson, J. Luo, and M. C. Wu, "A Large-Scale Microelectromechanical-Systems-Based Silicon Photonics Lidar," *Nature* 603, no. 7900 (2022): 253–258, https://doi.org/10.1038/s41586-022-04415-8.
- 34. D. Li, T. Ji, Y. Sun, et al., "A Full-Range Proximity-Tactile Sensor Based on Multimodal Perception Fusion for Minimally Invasive Surgical Robots," *Advanced Science* 12, no. 30 (2025): e02353, https://doi.org/10.1002/advs.202502353.
- 35. Z. Tong, H. Hu, Z. Wu, et al., "An Ultrasonic Proximity Sensing Skin for Robot Safety Control by Using Piezoelectric Micromachined Ultrasonic Transducers (Pmuts)," *IEEE Sensors Journal* 22, no. 18 (2022): 17351–17361, https://doi.org/10.1109/jsen.2021.3068487.
- 36. R. Wang, C. Li, H. Lyu, G. Pang, H. Wu, and G. Yang, "A Smooth Velocity Transition Framework Based on Hierarchical Proximity Sensing for Safe Human-Robot Interaction," *IEEE Robotics and Automation Letters* 9, no. 6 (2024): 4910–4917, https://doi.org/10.1109/lra. 2024.3385608.
- 37. W. Liu, F. Xiang, D. Mei, and Y. Wang, "A Flexible Dual-Mode Capacitive Sensor for Highly Sensitive Touchless and Tactile Sensing

- in Human-Machine Interactions," *Advanced Materials Technologies* 9, no. 4 (2023): 2301685, https://doi.org/10.1002/admt.202301685.
- 38. L. Bascetta, G. Magnani, P. Rocco, R. Migliorini, and M. Pelagatti, "Anti-Collision Systems for Robotic Applications Based on Laser Time-of-Flight sensors," in 2010 IEEE/ASME International Conference on Advanced Intelligent Mechatronics (IEEE, 2010), 278–284, https://doi.org/10.1109/AIM.2010.5695851.
- 39. X. Chen, M. Zhao, L. Xiang, et al., "Development of a Low-Cost Ultra-Tiny Line Laser Range Sensor," in 2016 IEEE/RSJ International Conference on Intelligent Robots and Systems (IROS) (IEEE, 2016), 111–116. https://doi.org/10.1109/IROS.2016.7759042.
- 40. D. Yang, Y. Liu, Q. Chen, et al., "Development of the High Angular Resolution 360° Lidar Based on Scanning MEMS Mirror," *Scientific Reports* 13, no. 1 (2023): 1540, https://doi.org/10.1038/s41598-022-26394-6.
- 41. P. Zolfaghari, M. Khodapanahandeh, H. Urey, and O. Ferhanoglu, "Cascaded Laser Scanning Towards High-Resolution LiDAR," *Optics & Laser Technology*, 168 (2024), https://doi.org/10.1016/j.optlastec.2023. 109906.
- 42. G. Luo, K. He, Y. Wang, et al., "Small Blind-Area, High-Accuracy Ultrasonic Rangefinder Using a Broadband Multi-Frequency Piezo-electric Micromachined Ultrasonic Transducer Array," *Measurement Science and Technology* 34, no. 12 (2023): 125140, https://doi.org/10.1088/1361-6501/acf682.
- 43. Y. Zhao, Z. Li, L. Liu, and M. Q. H.-Meng, "Robotically Steerable Intraluminal Imaging Probe With Side-Viewing 3D Photoacoustic Computed Tomography," *Optics Letters* 49, no. 21 (2024): 6089, https://doi.org/10.1364/ol.539670.
- 44. Z. Liu, D. Chen, J. Ma, T. Wang, D. Jia, and Y. Liu, "Multimodal Capacitive Proximity Sensing Array With Programmable Spatial Resolution and Dynamic Detection Range," *Sensors and Actuators A: Physical* 370 (2024): 115279, https://doi.org/10.1016/j.sna.2024.115279.
- 45. V. Sakthivelpathi, T. Li, Z. Qian, C. Lee, Z. Taylor, and J.-H. Chung, "Advancements and Applications of Micro and Nanostructured Capacitive Sensors: A Review," *Sensors and Actuators A: Physical* 377 (2024): 115701, https://doi.org/10.1016/j.sna.2024.115701.
- 46. Y. Li, X. Zhou, J. Chen, et al., "Laser-Patterned Copper Electrodes for Proximity and Tactile Sensors," *Advanced Materials Interfaces* 7, no. 4 (2020): 1901845, https://doi.org/10.1002/admi.201901845.
- 47. R. Mukhiya, P. Agarwal, S. Badjatya, et al., "Design, Modelling and System Level Simulations of DRIE-Based MEMS Differential Capacitive Accelerometer," *Microsystem Technologies* 25, no. 9 (2019): 3521–3532, https://doi.org/10.1007/s00542-018-04292-0.
- 48. P. Chabbi and V. K. P. Rao, "Coupled Field Simulation of MEMS Tuning Fork Gyroscope," in *Proceedings of ISSS International Conference on Micro, Nano, and Smart Systems*, ed. A. K. Pandey, M. Shojaei Baghini, and G. K. Ananthasuresh (Springer Nature Singapore, 2025), 271–277, https://doi.org/10.1007/978-981-96-3445-3_29.
- 49. D. Paci, A. Cantoni, G. Allegato, "Magnetometers," in *Silicon Sensors and Actuators*, ed. B. Vigna, P. Ferrari, F. F. Villa, E. Lasalandra, S. Zerbini (Springer, 2022), https://doi.org/10.1007/978-3-030-80135-9_14.
- 50. S. Fuller, Z. Yu, and Y. P. Talwekar, "A Gyroscope-Free Visual-Inertial Flight Control and Wind Sensing System for 10-mg Robots," *Science Robotics* 7, no. 72 (2022): eabq8184, https://doi.org/10.1126/scirobotics.abq8184.
- 51. T. S. Vaquero, G. Daddi, R. Thakker, et al., "EELS: Autonomous Snake-Like Robot With Task and Motion Planning Capabilities for Ice World Exploration," *Science Robotics* 9, no. 88 (2024): eadh8332, https://doi.org/10.1126/scirobotics.adh8332.
- 52. K. Liu, M. Ding, B. Pan, et al., "A Maneuverable Underwater Vehicle for Near-Seabed Observation," *Nature Communications* 15, no. 1 (2024): 10284, https://doi.org/10.1038/s41467-024-54600-8.

- 53. H. Ma, A. Song, J. Li, L. Ge, C. Fu, and G. Zhang, "Legged Odometry Based on Fusion of Leg Kinematics and IMU Information in a Humanoid Robot," *Biomimetic Intelligence and Robotics* 5, no. 1 (2025): 100196, https://doi.org/10.1016/j.birob.2024.100196.
- 54. X. Zhang, X. Huang, K. Hong, Q. Li, R. Wang, and B. Zhou, "TUC-Net: A Point Cloud Segmentation Network Based on Neighborhood Feature Perception Aggregation for Tunnels Under Construction," *IEEE Transactions on Intelligent Transportation Systems* 26, no. 7 (2025): 10048–10066, https://doi.org/10.1109/tits.2025.3542500.
- 55. W. Babatain, S. Bhattacharjee, A. M. Hussain, and M. M. Hussain, "Acceleration Sensors: Sensing Mechanisms, Emerging Fabrication Strategies, Materials, and Applications," *ACS Applied Electronic Materials* 3, no. 2 (2021): 504–531, https://doi.org/10.1021/acsaelm.0c00746.
- 56. L. Zhong, L. Xue, X. Deng, S. Liu, and Z. Zhu, "High Power-Efficiency Readout Circuit for MEMS Capacitive Accelerometer," *IEEE Transactions on Circuits and Systems II: Express Briefs* 71, no. 1 (2024): 76–80, https://doi.org/10.1109/tcsii.2023.3304636.
- 57. C.-H. Peng and M. S.-C. Lu, "Design and Characterization of CMOS Micromachined Piezoresistive Accelerometers," *IEEE Sensors Journal* 24, no. 3 (2024): 2500–2506, https://doi.org/10.1109/jsen.2023.3340864.
- 58. Y. Liu, Y. Yuan, Y. Gong, et al., presented at 2024 IEEE Sensors, (2024).
- 59. Z. Fang, Y. Yin, C. Chen, S. Zhang, Y. Liu, and F. Han, "A Sensitive Micromachined Resonant Accelerometer for Moving-Base Gravimetry," *Sensors and Actuators A: Physical* 325 (2021): 112694, https://doi.org/10.1016/j.sna.2021.112694.
- 60. X. Ren, X. Zhou, S. Yu, X. Wu, and D. Xiao, "Frequency-Modulated MEMS Gyroscopes: A Review," *IEEE Sensors Journal* 21, no. 23 (2021): 26426–26446, https://doi.org/10.1109/jsen.2021.3117939.
- 61. Y. Jung, E. Jo, and J. Kim, "Electrostatically Driven Two-Axis Microelectromechanical Magnetometer With Eccentric Resonator and Electromagnetic Inductor," *Sensors and Actuators A: Physical* 387 (2025): 116378, https://doi.org/10.1016/j.sna.2025.116378.
- 62. H. Zhang, X. Wei, Y. Ding, Z. Jiang, and J. Ren, "A Low Noise Capacitive MEMS Accelerometer With Anti-Spring Structure," *Sensors and Actuators A: Physical* 296 (2019): 79–86, https://doi.org/10.1016/j.sna.2019.06.051.
- 63. T. Kim, S. Jang, B. Chang, et al., "A New Simple Fabrication Method for Silicon Nanowire-Based Accelerometers," in 2019 20th International Conference on Solid-State Sensors, Actuators and Microsystems & Eurosensors XXXIII (TRANSDUCERS & EUROSENSORS XXXIII) (2019), 1949–1952, https://doi.org/10.1109/TRANSDUCERS.2019.8808764.
- 64. M.-h. Xu, H. Zhou, L.-h. Zhu, et al., "Design and Fabrication of a D33-Mode Piezoelectric Micro-Accelerometer," *Microsystem Technologies* 25, no. 12 (2019): 4465–4474, https://doi.org/10.1007/s00542-019-04495-z.
- 65. Z. Qi, B. Wang, Z. Zhai, et al., "Bridging Piezoelectric and Electrostatic Effects: A Novel Piezo-MEMS Pitch/Roll Gyroscope With Sub 10°/h Bias Instability," *Microsystems & Nanoengineering* 10, no. 160 (2024), https://doi.org/10.1038/s41378-024-00773-7.
- 66. J. Yu, P. Cai, and H. Liang, "A Lorentz-Force MEMS Magnetometer With an Annular Resonance Beam for Z-Axis Sensing," *IEEE Sensors Journal* 25, no. 2 (2025): 2502–2509, https://doi.org/10.1109/jsen.2024. 3508068.
- 67. H. Yousef, M. Boukallel, and K. Althoefer, "Tactile Sensing for Dexterous in-Hand Manipulation in Robotics—A Review," *Sensors and Actuators A: Physical* 167, no. 2 (2011): 171–187, https://doi.org/10.1016/j.sna.2011.02.038.
- 68. D. Li, A. Li, Z. Zhang, T. Ji, K. Wang, and H. Liu, "Highly Sensitive MEMS Three-Dimensional Force Sensor for Robot-Assisted Minimally Invasive Surgery," *Science China Technological Sciences* 68, no. 9 (2025): 1920301, https://doi.org/10.1007/s11431-025-2986-8.

- 69. C. Hou, H. Gao, X. Yang, et al., "A Piezoresistive-Based 3-Axial MEMS Tactile Sensor and Integrated Surgical Forceps for Gastrointestinal Endoscopic Minimally Invasive Surgery," *Microsystems & Nanoengineering* 10, (2024): 141, https://doi.org/10.1038/s41378-024-00774-6.
- 70. U. Kim, Y. B. Kim, J. So, D.-Y. Seok, and H. R. Choi, "Sensorized Surgical Forceps for Robotic-Assisted Minimally Invasive Surgery," *IEEE Transactions on Industrial Electronics* 65, no. 12 (2018): 9604–9613, https://doi.org/10.1109/tie.2018.2821626.
- 71. U. Kim, Y. B. Kim, D.-Y. Seok, J. So, and H. R. Choi, "A Surgical Palpation Probe With 6-Axis Force/Torque Sensing Capability for Minimally Invasive Surgery," *IEEE Transactions on Industrial Electronics* 65, no. 3 (2018): 2755–2765, https://doi.org/10.1109/tie.2017. 2739681
- 72. C. Ge, B. Yang, L. Wu, et al., "Capacitive Sensor Combining Proximity and Pressure Sensing for Accurate Grasping of a Prosthetic Hand," *ACS Applied Electronic Materials* 4, no. 2 (2022): 869–877, https://doi.org/10.1021/acsaelm.1c01274.
- 73. M. Muroyama, H. Hirano, C. Shao, and S. Tanaka, "Development of a Real-Time Force and Temperature Sensing System With MEMS-LSI Integrated Tactile Sensors for Next-Generation Robots," *Journal of Robotics and Mechatronics* 32, no. 2 (2020): 323–332, https://doi.org/10.20965/jrm.2020.p0323.
- 74. Z. Gong, Z. Gao, G. Zhu, and T. Zhang, "A Solid-Liquid Composite Flexible Bionic Three-Axis Tactile Sensor for Dexterous Hands," *IEEE Robotics and Automation Letters* 9 (2024): 7907–7914, https://doi.org/10.1109/lra.2024.3433203.
- 75. X. Hu, C. Jiang, B. Yang, and J. Liu, "A Visual-Tactile Coulping Mechanism Sensor For Real-Time Force Calibration," in 2024 IEEE 37th International Conference on Micro Electro Mechanical Systems (MEMS), (IEEE, 2024), 825–828, https://doi.org/10.1109/mems58180.2024.10439598.
- 76. Y. Yu, J. Li, S. A. Solomon, et al., "All-Printed Soft Human-Machine Interface for Robotic Physicochemical Sensing," *Science Robotics* 7, no. 67 (2022): eabn0495, https://doi.org/10.1126/scirobotics.abn0495.
- 77. F. Liu, S. Deswal, A. Christou, Y. Sandamirskaya, M. Kaboli, and R. Dahiya, "Neuro-Inspired Electronic Skin for Robots," *Science Robotics* 7, no. 67 (2022): eabl7344, https://doi.org/10.1126/scirobotics.abl7344.
- 78. Z. Chen, J. Du, Y. Wang, et al., "Fully Integrated Multifunctional Flexible Ultrasonic-Electric-Coupled Patches for Advancing Wound Care Paradigms," *Advanced Functional Materials* 35, no. 24 (2025): 2425025, https://doi.org/10.1002/adfm.202425025.
- 79. Y. Xi, P. Tan, Z. Li, and Y. Fan, "Self-Powered Wearable Iot Sensors as Human-Machine Interfaces," *Soft Science* 3 (2023), https://doi.org/10.20517/ss.2023.13.
- 80. Y. Luo, X. Chen, X. Li, H. Tian, L. Wang, and J. Shao, "A Flexible Dual-Function Capacitive Sensor Enhanced by Loop-Patterned Fibrous Electrode and Doped Dielectric Pillars for Spatial Perception," *Nano Research* 16, no. 5 (2023): 7550–7558, https://doi.org/10.1007/s12274-022-5309-z.
- 81. X. Zhao, Z. Sun, and C. Lee, "Augmented Tactile Perception of Robotic Fingers Enabled by Ai-Enhanced Triboelectric Multimodal Sensors," *Advanced Functional Materials* 34, no. 49 (2024): 2409558, https://doi.org/10.1002/adfm.202409558.
- 82. Y. Chen, T. Li, Z. Wang, Z. Yan, R. De Vita, and T. Tan, "A Metamaterial Computational Multi-Sensor of Grip-Strength Properties With Point-Of-Care Human-Computer Interaction," *Advanced Science* 10, no. 34 (2023): 2304091, https://doi.org/10.1002/advs.202304091.
- 83. M. Cai, Z. Jiao, S. Nie, C. Wang, J. Zou, and J. Song, "A Multifunctional Electronic Skin Based on Patterned Metal Films for Tactile Sensing With a Broad Linear Response Range," *Science Advances* 7, no. 52 (2021): eabl8313, https://doi.org/10.1126/sciadv.abl8313.
- 84. C. M. Boutry, M. Negre, M. Jorda, et al., "A Hierarchically Patterned, Bioinspired E-Skin Able to Detect the Direction of Applied

- Pressure for Robotics," *Science Robotics* 3, no. 24 (2018), https://doi.org/10.1126/scirobotics.aau6914.
- 85. D. Kong, Y. Lu, S. Zhou, et al., "Super-Resolution Tactile Sensor Arrays With Sparse Units Enabled by Deep Learning," *Science Advances* 11, no. 27 (2025): eadv2124, https://doi.org/10.1126/sciadv.adv2124.
- 86. G. Li, S. Liu, L. Wang, and R. Zhu, "Skin-Inspired Quadruple Tactile Sensors Integrated on a Robot Hand Enable Object Recognition," *Science Robotics* 5, no. 49 (2020): eabc8134, https://doi.org/10.1126/scirobotics.abc8134.
- 87. N. Bai, Y. Xue, S. Chen, et al., "A Robotic Sensory System With High Spatiotemporal Resolution for Texture Recognition," *Nature Communications* 14, no. 1 (2023): 7121, https://doi.org/10.1038/s41467-023-42722-4.
- 88. X. Guo, Z. Sun, Y. Zhu, and C. Lee, "Zero-Biased Bionic Fingertip E-Skin With Multimodal Tactile Perception and Artificial Intelligence for Augmented Touch Awareness," *Advanced Materials* 36, no. 39 (2024): 2406778, https://doi.org/10.1002/adma.202406778.
- 89. Y. Sun, T. Chen, D. Li, et al., "Stretchable, Multiplexed, and Bimodal Sensing Electronic Armor for Colonoscopic Continuum Robot Enhanced by Triboelectric Artificial Synapse," *Advanced Materials* 37, no. 33 (2025): e2502203, https://doi.org/10.1002/adma.202502203.
- 90. B. Dai, Y. Zheng, Y. Qian, et al., "An Optical/Electronic Artificial Skin Extends the Robotic Sense to Molecular Sensing," *NPJ Flexible Electronics* 9, no. 1 (2025): 87, https://doi.org/10.1038/s41528-025-00431-6.
- 91. S. J. Hong, Y. R. Lee, A. Bag, et al., "Bio-Inspired Artificial Mechanoreceptors With Built-in Synaptic Functions for Intelligent Tactile Skin," *Nature Materials* 24, no. 7 (2025): 1100–1108, https://doi.org/10.1038/s41563-025-02204-y.
- 92. Q. Mao, Z. Liao, S. Liu, J. Yuan, and R. Zhu, "An Ultralight, Tiny, Flexible Six-Axis Force/Torque Sensor Enables Dexterous Fingertip Manipulations," *Nature Communications* 16, no. 1 (2025): 5693, https://doi.org/10.1038/s41467-025-60861-8.
- 93. Z. Sun, T. He, Z. Ren, et al., "Moving Toward Human-Like Perception and Sensation Systems—From Integrated Intelligent Systems to Decentralized Smart Devices," *SmartSys* 1 (2025): e4, https://doi.org/10.1002/sys3.4.
- 94. X. Zhang, H. Chen, J. Xu, X. Song, J. Wang, and X. Chen, "A Novel Sound-Based Belt Condition Monitoring Method for Robotic Grinding Using Optimally Pruned Extreme Learning Machine," *Journal of Materials Processing Technology* 260 (2018): 9–19, https://doi.org/10.1016/j.jmatprotec.2018.05.013.
- 95. Q. Zhang, Y. Wang, D. Li, et al., "Flexible Multifunctional Platform Based on Piezoelectric Acoustics for Human–Machine Interaction and Environmental Perception," *Microsystems & Nanoengineering* 8, no. 1, https://doi.org/10.1038/s41378-022-00402-1.
- 96. J. Chang, T. Maltby, A. Moineddini, et al., "Piezoelectric Nanofiber-Based Intelligent Hearing System," *Science Advances* 11, no. 19 (2025): eadl2741, https://doi.org/10.1126/sciadv.adl2741.
- 97. W.-T. Shih, W.-H. Tsou, D. Vasic, F. Costa, and W.-J. Wu, "The Woofer-Type Piezo-Actuated Microspeaker Based on Aerosol Deposition and Metal MEMS Process," *Micromachines* 16, no. 3 (2025): 353, https://doi.org/10.3390/mi16030353.
- 98. C. Sun, J. Sang, Z. Duanmu, B. Liu, and X. Li, "Sensitivity Analysis for Dual-Membrane Capacitive MEMS Microphone," *IEEE Sensors Journal* 24, no. 15 (2024): 24015–24022, https://doi.org/10.1109/jsen. 2024.3417384.
- 99. S. A. Zawawi, A. A. Hamzah, B. Y. Majlis, and F. Mohd-Yasin, "A Review of MEMS Capacitive Microphones," *Micromachines*, 11, no. 5 (2020): 484, https://doi.org/10.3390/mi11050484.
- 100. M. Khatib and H. Haick, "Sensors for Volatile Organic Compounds," *ACS Nano* 16, no. 5 (2022): 7080–7115, https://doi.org/10.1021/acsnano.1c10827.

- 101. Y. Xia, S. Guo, L. Yang, et al., "Enhanced Free-Radical Generation on MoS₂/Pt by Light and Water Vapor Co-Activation for Selective CO Detection With High Sensitivity," *Advanced Materials* 35, no. 30 (2023): 2303523, https://doi.org/10.1002/adma.202303523.
- 102. R. A. Potyrailo, S. Go, D. Sexton, et al., "Extraordinary Performance of Semiconducting Metal Oxide Gas Sensors Using Dielectric Excitation," *Nature Electronics* 3, no. 5 (2020): 280–289, https://doi.org/10.1038/s41928-020-0402-3.
- 103. I. A. Kalinin, I. V. Roslyakov, D. Bograchev, et al., "High Performance Microheater-Based Catalytic Hydrogen Sensors Fabricated on Porous Anodic Alumina Substrates," *Sensors and Actuators B: Chemical* 404 (2024): 135270, https://doi.org/10.1016/j.snb.2023.135270.
- 104. Z. Huang, W. Yang, Y. Zhang, et al., "Miniaturized Electrochemical Gas Sensor With a Functional Nanocomposite and Thin Ionic Liquid Interface for Highly Sensitive and Rapid Detection of Hydrogen," *Analytical Chemistry* 96, no. 45 (2024): 17960–17968, https://doi.org/10.1021/acs.analchem.4c02561.
- 105. I. Kim, W.-S. Kim, K. Kim, et al., "Holographic Metasurface Gas Sensors for Instantaneous Visual Alarms," *Science Advances* 7, no. 15 (2021): eabe9943, https://doi.org/10.1126/sciadv.abe9943.
- 106. K. Persaud and G. Dodd, "Analysis of Discrimination Mechanisms in the Mammalian Olfactory System Using a Model Nose," *Nature* 299, no. 5881 (1982): 352–355, https://doi.org/10.1038/299352a0.
- 107. D. Li, Z. Xie, M. Qu, Q. Zhang, Y. Fu, and J. Xie, "Virtual Sensor Array Based on Butterworth-Van Dyke Equivalent Model of QCM for Selective Detection of Volatile Organic Compounds," *ACS Applied Materials & Interfaces* 13, no. 39 (2021): 47043–47051, https://doi.org/10.1021/acsami.1c13046.
- 108. D. Li, B. Zhu, K. Pang, et al., "Virtual Sensor Array Based on Piezoelectric Cantilever Resonator for Identification of Volatile Organic Compounds," *ACS Sensors* 7, no. 5 (2022): 1555–1563, https://doi.org/10.1021/acssensors.2c00442.
- 109. X. Chen and J. Huang, "Combining Particle Filter Algorithm With Bio-Inspired Anemotaxis Behavior: A Smoke Plume Tracking Method and Its Robotic Experiment Validation," *Measurement* 154 (2020): 107482, https://doi.org/10.1016/j.measurement.2020.107482.
- 110. R. A. Potyrailo, "Multivariable Sensors for Ubiquitous Monitoring of Gases in the Era of Internet of Things and Industrial Internet," *Chemical Reviews* 116, no. 19 (2016): 11877–11923, https://doi.org/10.1021/acs.chemrev.6b00187.
- 111. H. Ishida, K. Suetsugu, T. Nakamoto, and T. Moriizumi, "Study of Autonomous Mobile Sensing System for Localization of Odor Source Using Gas Sensors and Anemometric Sensors," *Sensors and Actuators A: Physical* 45, no. 2 (1994): 153–157, https://doi.org/10.1016/0924-4247(94) 00829-9.
- 112. A. T. Hayes, A. Martinoli, and R. M. Goodman, *Proceedings 2001 IEEE/RSJ International Conference on Intelligent Robots and Systems. Expanding the Societal Role of Robotics in the the next Millennium*, Vol. 2, 2001), 1073–1078: *Cat. No.01CH37180*).
- 113. C. Bartolozzi, G. Indiveri, and E. Donati, "Embodied Neuromorphic Intelligence," *Nature Communications* 13, no. 1 (2022): 1024, https://doi.org/10.1038/s41467-022-28487-2.
- 114. M. Kathiresan, C. Manikandan, S. Premkumar, et al., "Key Issues and Challenges in Device Level Fabrication of MEMS Acoustic Sensors Using Piezo Thin Films Doped With Strontium and Lanthanum," *Journal of Materials Science: Materials in Electronics* 33, no. 14 (2022): 11271–11280, https://doi.org/10.1007/s10854-022-08102-2.
- 115. P. Singh and S. Kumar, "Laser-Assisted Stress Reduction in Molybdenum Microstructures for CMOS Compatible MEMS Integration," *Sensors and Actuators A: Physical* 295 (2019): 523–531, https://doi.org/10.1016/j.sna.2019.05.020.

- 116. X. Liu, S. Wen, J. Zhao, T. Z. Qiu, and H. Zhang, "Edge-Assisted Multi-Robot Visual-Inertial SLAM With Efficient Communication," *IEEE Transactions on Automation Science and Engineering* 22 (2025): 2186–2198, https://doi.org/10.1109/tase.2024.3376427.
- 117. J. Moon, D. Hong, J. Kim, et al., "Enhancing Autonomous Driving Robot Systems With Edge Computing and LDM Platforms," *Electronics* 13, no. 14 (2024): 2740, https://doi.org/10.3390/electronics13142740.
- 118. N. Gupta, A. Khandelwal, and S. Maheshwari, "Microheater Material Selection Framework for Micro-Electromechanical System (MEMS)-Based Gas Sensor," *IEEE Sensors Journal* 23, no. 22 (2023): 27096–27101, https://doi.org/10.1109/jsen.2023.3318574.
- 119. Y. Long, Z. Liu, and F. Ayazi, "4H-Silicon Carbide as an Acoustic Material for MEMS," *IEEE Transactions on Ultrasonics, Ferroelectrics, and Frequency Control* 70, no. 10 (2023): 1189–1200, https://doi.org/10.1109/tuffc.2023.3282920.
- 120. C. Zhang, Y. Liu, M. Wu, and N. Liao, "Experiment Research on Micro-/Nano Processing Technology of Graphite as Basic MEMS Material," *Applied Sciences* 9, no. 15 (2019): 3103, https://doi.org/10.3390/app9153103.
- 121. S. Xu and Z. Wu, "Adaptive Learning Control of Robot Manipulators via Incremental Hybrid Neural Network," *Neurocomputing* 568 (2024): 127045, https://doi.org/10.1016/j.neucom.2023.127045.
- 122. S. Duan, Q. Shi, and J. Wu, "Multimodal Sensors and Ml-Based Data Fusion for Advanced Robots," *Advanced Intelligent Systems* 4, no. 12 (2022): 2200213, https://doi.org/10.1002/aisy.202200213.
- 123. W. Qi, H. Fan, H. R. Karimi, and H. Su, "An Adaptive Reinforcement Learning-Based Multimodal Data Fusion Framework for Human–Robot Confrontation Gaming," *Neural Networks* 164 (2023): 489–496, https://doi.org/10.1016/j.neunet.2023.04.043.
- 124. J. Guo, F. Guo, H. Zhao, et al., "In-Sensor Computing With Visual-Tactile Perception Enabled by Mechano-Optical Artificial Synapse," *Advanced Materials* 37, no. 14 (2025): 2419405, https://doi.org/10.1002/adma.202419405.
- 125. K. Kimizuka, S. Azhari, S. Tokuno, et al., "Haptic In-Sensor Computing Device Based on CNT/PDMS Nanocomposite Physical Reservoir," *Advanced Intelligent Systems* 7, no. 3 (2025): 2400640, https://doi.org/10.1002/aisy.202400640.
- 126. H. Qiu, Z. Chen, Y. Chen, et al., "A Real-Time Hand Gesture Recognition System for Low-Latency HMI via Transient HD-SEMG and In-Sensor Computing," *IEEE Journal of Biomedical and Health Informatics* 28, no. 9 (2024): 5156–5167, https://doi.org/10.1109/jbhi.2024. 3417236.
- 127. Y. Cai, Y. Zhao, W. Zhang, and N. Xing, "The Multi-Modal Robot Perception, Language Information, and Environment Prediction Model Based on Deep Learning," *Journal of Organizational and End User Computing* 36 (2024): 1–21, https://doi.org/10.4018/joeuc.349987.
- 128. H. Zeng and J. Luo, "Construction of Multi-Modal Perception Model of Communicative Robot in Non-Structural Cyber Physical System Environment Based on Optimized BT-SVM Model," *Computer Communications* 181 (2022): 182–191, https://doi.org/10.1016/j.comcom.2021. 10.019.